Molecular crosstalk between Y5 receptor and neuropeptide Y drives liver cancer

Peter Dietrich,[1,2] Laura Wormser,[1] Valerie Fritz,[1] Tatjana Seitz,[1] Monica De Maria,[3] Alexandra Schambony,[3] Andreas E. Kremer,[2] Claudia Günther,[2] Timo Itzel,[4] Wolfgang E. Thasler,[5] Andreas Teufel,[4] Jonel Trebicka,[6] Arndt Hartmann,[7,8] Markus F. Neurath,[2,8] Stephan von Hörsten,[9] Anja K. Bosserhoff,[1,8] and Claus Hellerbrand[1,8]

[1]Institute of Biochemistry, Emil-Fischer-Zentrum, [2]Department of Medicine 1, University Hospital Erlangen, and [3]Biology Department, Developmental Biology, Friedrich-Alexander University Erlangen-Nürnberg, Erlangen, Germany. [4]Department of Internal Medicine II, Medical Faculty Mannheim, Heidelberg University, Mannheim, Germany. [5]Hepacult GmbH, Planegg, Germany. [6]Department of Medicine I, University Hospital Bonn, Bonn, Germany. [7]Institute of Pathology, Friedrich-Alexander University Erlangen-Nürnberg, Erlangen, Germany. [8]Comprehensive Cancer Center Erlangen–European Metropolitan Region of Nuremberg, Erlangen, Germany. [9]Department of Experimental Therapy, Franz Penzoldt Center, Friedrich-Alexander University Erlangen-Nürnberg, Erlangen, Germany.

Hepatocellular carcinoma (HCC) is clearly age-related and represents one of the deadliest cancer types worldwide. As a result of globally increasing risk factors including metabolic disorders, the incidence rates of HCC are still rising. However, the molecular hallmarks of HCC remain poorly understood. Neuropeptide Y (NPY) and NPY receptors represent a highly conserved, stress-activated system involved in diverse cancer-related hallmarks including aging and metabolic alterations, but its impact on liver cancer had been unclear. Here, we observed increased expression of NPY5 receptor (Y5R) in HCC, which correlated with tumor growth and survival. Furthermore, we found that its ligand NPY was secreted by peritumorous hepatocytes. Hepatocyte-derived NPY promoted HCC progression by Y5R activation. TGF-β1 was identified as a regulator of NPY in hepatocytes and induced Y5R in invasive cancer cells. Moreover, NPY conversion by dipeptidylpeptidase 4 (DPP4) augmented Y5R activation and function in liver cancer. The TGF-β/NPY/Y5R axis and DPP4 represent attractive therapeutic targets for controlling liver cancer progression.

Introduction

Hepatocellular carcinoma (HCC) is the fourth most common cause of cancer-related mortality worldwide and one of the cancers with still-increasing incidence rates (1). Major risk factors are chronic infection with hepatitis B and C viruses and alcohol abuse (1). However, nonalcoholic fatty liver disease (NAFLD), which is associated with obesity, insulin resistance, and type 2 diabetes, also represents an increasingly recognized trigger for HCC development, especially in developed countries (1, 2). In this context, advanced age has been reported to predispose to HCC, and indeed, HCC is mainly affecting those of age 65 years and older (3). Likewise, aging is recognized as a significant and independent risk factor for cancer (4, 5). Hallmarks of cancer development and progression resemble hallmarks of aging, including cellular stress, autophagy, and deregulated nutrient sensing, which is correlated with metabolic disorders such as obesity, insulin resistance, and NAFLD (6, 7).

Human aging is tightly linked to activation of the stress-induced sympathoadrenergic system (8, 9). Moreover, sympathoadrenergic signaling has emerged as a strong promoter of several cancer types (10–13). Sympathoadrenergic effects are mediated by catecholamines and the highly conserved neuropeptide Y (NPY). NPY is one of the most widely expressed neurotransmitters in the central and peripheral nervous systems (14). NPY signals via binding and activation of the G protein–coupled receptors Y1R, Y2R, and Y5R (15). Thus, NPY plays a crucial role in various biological processes, including cortical excitability, stress response, food intake, circadian rhythms, and cardiovascular function (16). Several milestone studies also suggested key roles of the NPY system in the regulation of diverse common hallmarks of aging, metabolic disorders, and cancer (17), including autophagy (18), nutrient sensing, caloric restriction, appetite regulation (19–21), mitochondrial dysfunction (22), cell proliferation (23), and hematopoietic stem and progenitor cell properties like migration and intra-/extravasation (24).

With regard to the liver, systemic NPY levels have been described as potent modulators of chronic liver disease (25–28). NPY affects hepatic lipid and glucose metabolism in a way that favors the development of hepatic steatosis, and knockdown of NPY in the hypothalamus promotes hepatic insulin sensitivity in rats (29). Accordingly, transgenic overexpression of NPY in noradrenergic neurons increased hepatic levels of triglycerides and cholesterol in mice (30). Furthermore, NPY controls hepatic VLDL-triglyceride secretion via the sympathetic nervous system (31). Moreover, an in vitro study revealed that NPY promoted the proliferation of activated hepatic stellate cells, which could impact hepatic fibrosis (28). Further studies demonstrated pronounced

Authorship note: AKB and CH contributed equally to this work.
Conflict of interest: The authors have declared that no conflict of interest exists.

Submitted: July 18, 2019; **Accepted:** January 23, 2020; **Published:** April 13, 2020.
Reference information: *J Clin Invest*. 2020;130(5):2509–2526.
https://doi.org/10.1172/JCI131919.

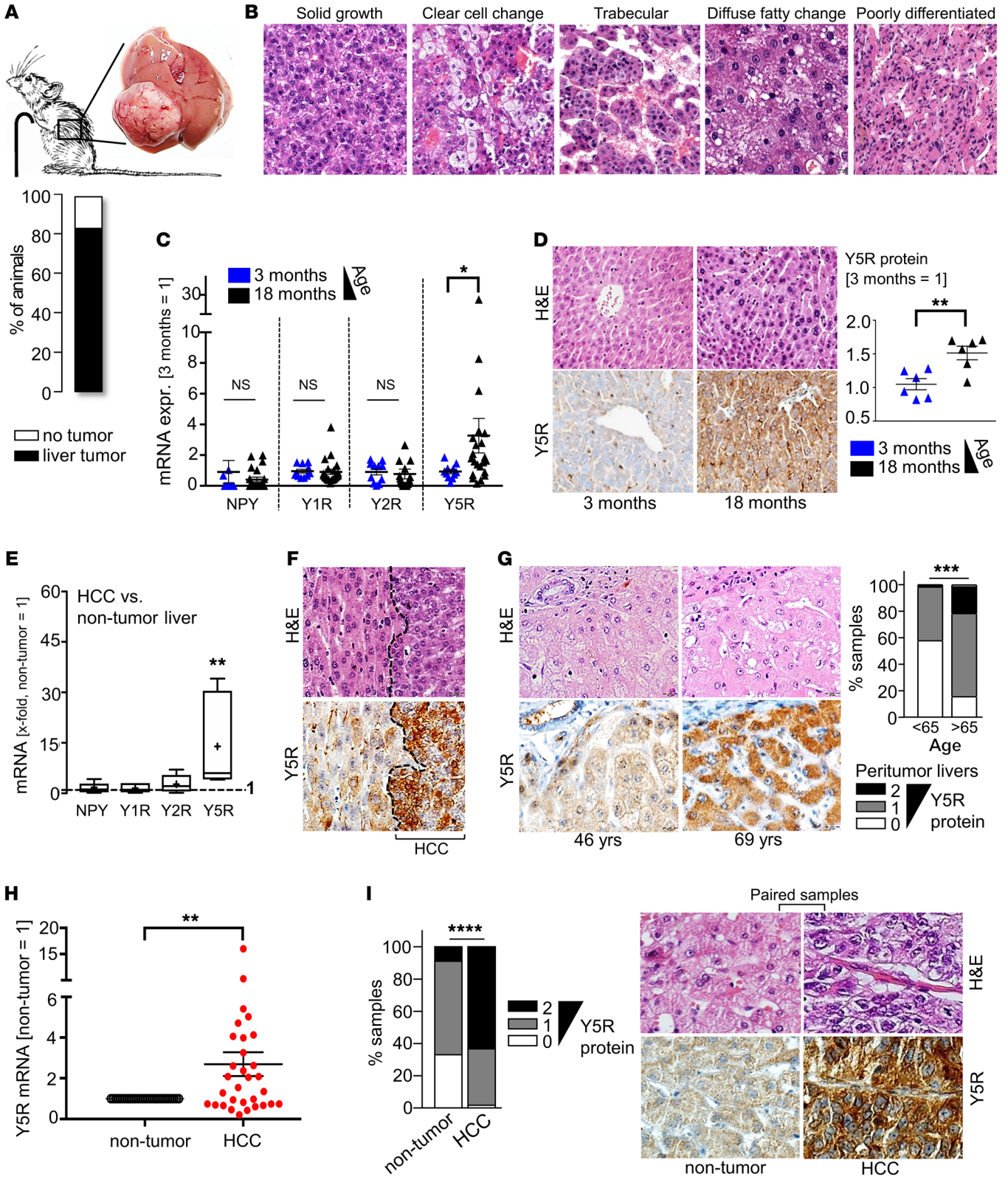
A
B
Solid growth
Clear cell change
Trabecular
Diffuse fatty change
Poorly differentiated
% of animals
no tumor
liver tumor
C
3 months
18 months
Age
mRNA expr. [3 months = 1]
NS
NPY
Y1R
Y2R
Y5R
D
H&E
Y5R
3 months
18 months
Y5R protein
[3 months = 1]
E
HCC vs.
non-tumor liver
mRNA [x-fold, non-tumor = 1]
F
HCC
G
46 yrs
69 yrs
% samples
<65
>65
Age
Peritumor livers
Y5R protein
H
Y5R mRNA [non-tumor = 1]
non-tumor
HCC
I
Paired samples
non-tumor
HCC

Figure 1. Upregulation of NPY5 receptor in HCC. (**A**) Explanted, tumor-bearing liver (representative image) derived from an aged C3H/HeN mouse, and bar graph (below) depicting percentages of tumor-bearing mice, age 18 months (n = 12). (**B**) Representative H&E staining (20-fold original magnification; n = 12) depicting histological heterogeneity of HCC derived from aged C3H mice. (**C**) Normalized mRNA levels of NPY, Y1R, Y2R, and Y5R in nontumorous livers comparing young (n = 11) with aged (n = 22) mice. (**D**) Representative images (10-fold original magnification; H&E and Y5R staining) and IHC analysis of Y5R levels in nontumorous livers comparing young (n = 6) and aged (n = 6) mice. (**E**) Normalized NPY, Y1R, Y2R, and Y5R mRNA levels in HCC compared with corresponding nontumorous liver tissues derived from aged C3H mice (n = 8) (box-and-whisker plots [minimum to maximum]; "+" indicates mean values). (**F**) Representative images (H&E and Y5R staining; 20-fold original magnification) of age-related HCC and peritumorous tissues derived from C3H mice (n = 12). (**G**) Representative images (H&E and Y5R staining; 40-fold original magnification); Y5R protein expression (IHC) in nontumorous liver tissues of younger (<65 years) (n = 57) compared with older (>65 years) (n = 51) HCC patients. (**H**) Y5R mRNA levels in paired HCC and corresponding peritumorous tissues (n = 31 pairs). (**I**) Representative images (H&E and Y5R staining; 40-fold original magnification) and IHC analysis of Y5R protein levels in HCC compared with corresponding peritumorous tissues (n = 231). Data are presented as mean ± SEM. Statistical significance was determined by 2-tailed, unpaired t test (**C** and **D**), 2-tailed, paired t test (**E** and **H**), 2-sided Fisher's exact test and Spearman's correlation (**G** and **I**), and uni- and multivariate analysis (ordinal regression analysis, link function: logit) (**G**). $^{*}P < 0.05$, $^{**}P < 0.01$, $^{***}P < 0.001$, $^{****}P < 0.0001$.

vasoactive effects of NPY in portal hypertension, which represents a life-threatening complication of advanced liver cirrhosis (25–27). However, the role of the NPY system in liver cancer remained elusive, and has now been addressed in this study.

Results

Enhanced NPY5 receptor expression in a spontaneous mouse model of liver cancer and in patients with HCC. Although spontaneous hepatocarcinogenesis in aged C3H/HeN mice was first described in 1960, the underlying mechanisms are still unknown (32–38). Since the NPY system was linked to hallmarks of aging, C3H/HeN mice were chosen as a model system to explore age-related gene expression patterns of the NPY system in hepatocarcinogenesis. Eighty percent of aged (>18 months) male C3H/HeN mice exhibited macroscopic liver tumors (Figure 1A). Histological analysis revealed diverse HCC-related growth patterns representing inter- and intratumorous heterogeneity as frequently observed in murine and human HCC (Figure 1B and refs. 39–41). Analysis of surrounding nontumorous liver tissue revealed that as compared with young mice, significantly higher NPY5 receptor (Y5R) mRNA expression was detected in aged mice, while Y1R, Y2R, and NPY expression levels showed no age-dependent differences (Figure 1C). Age-dependent upregulation of hepatic Y5R (but not Y1R and Y2R) mRNA levels was also found in Gene Expression Omnibus (GEO) data sets derived from mouse and rat models (Supplemental Figure 1, A and B; supplemental material available online with this article; https://doi.org/10.1172/JCI131919DS1; supplemental material available online with this article; https://doi.org/10.1172/JCI131919DS1). On the protein level, immunohistochemical (IHC) analysis confirmed higher Y5R expression in livers of aged as compared with young C3H/HeN mice (Figure 1D and Supplemental Figure 1C).

Strikingly, in HCC tissues of aged C3H/HeN mice, Y5R mRNA and protein levels were even further upregulated as compared with corresponding nontumorous liver tissues (Figure 1, E and F, and Supplemental Figure 1D), while no cancer-related upregulation was found for NPY, Y1R, and Y2R (Figure 1E).

Applying patient-derived samples, Y5R mRNA and protein expression levels were confirmed to be low in nontumorous liver tissues but also increased with age (Figure 1G; Supplemental Figure 1, E–G; and Supplemental Table 3). Moreover, Y5R mRNA levels were further upregulated in human HCC tissues (Figure 1H). Immunohistological analysis of a tissue microarray comprising paired samples of human HCC tissues and corresponding nontumorous liver samples of the same patient (42–44) confirmed strong expression and marked upregulation of Y5R protein expression in HCC (Figure 1I; Supplemental Figure 1, H and I; and Supplemental Table 1).

Overexpression of both mRNA and protein levels of Y5R pointed to transcriptional upregulation in HCC. Screening of the Catalogue of Somatic Mutations in Cancer (COSMIC) database revealed age-associated hypomethylation of a CpG island within the Y5R gene applying human HCC samples derived from The Cancer Genome Atlas (TCGA) (Supplemental Figure 1J). Further analysis (applying the MethHC database, ref. 45; and the same TCGA cohort) revealed age-related hypomethylation of 4 additional CpG sites within the Y5R promoter region, which was inversely correlated with Y5R expression (Supplemental Figure 1, K and L). These findings link age-dependent differential methylation of Y5R with enhanced gene expression in HCC. Alterations in DNA methylation have been described as a molecular link between aging and caner (46), were shown to occur in most cancer types, and can induce genomic instability and liver cancer formation (47–49).

According to these findings, the upregulation of Y5R expression in liver cancer prompted us to ask whether this NPY receptor might have functional impact in HCC.

Y5R enhances tumorigenicity of HCC and correlates with tumor progression and poor survival. Y5R was also strongly overexpressed in human HCC cell lines as compared with primary human hepatocytes (Figure 2, A and B). Its ligand NPY was abundantly detected in the serum that had been added to the cell culture medium for functional in vitro analysis (Supplemental Figure 2A). siRNA pool–mediated knockdown of Y5R (Supplemental Figure 2B) induced strong reduction of Ki-67 expression and proliferation in HCC cells (Figure 2, C and D, and Supplemental Figure 2C). Fitting with these in vitro findings, Y5R expression levels correlated with cyclin D1 and Ki-67 expression in HCC tissues (Figure 2E and Supplemental Figure 2D). Furthermore, Y5R knockdown markedly reduced both number and size of colonies formed by HCC cells according to clonogenicity assays (Figure 2F and Supplemental Figure 2E). Stem cell properties including enhanced clonogenicity are well known to contribute to HCC development and progression (50).

Analysis of several different TCGA data sets revealed enhanced Y5R expression in high-risk compared with low-risk (based on prognostic index) HCC patient groups. Furthermore, high Y5R expression was also associated with poor overall and recurrence-free survival (Figure 2G and Supplemental Figure 2F) as well as with advanced tumor stages (Supplemental Figure 2G)

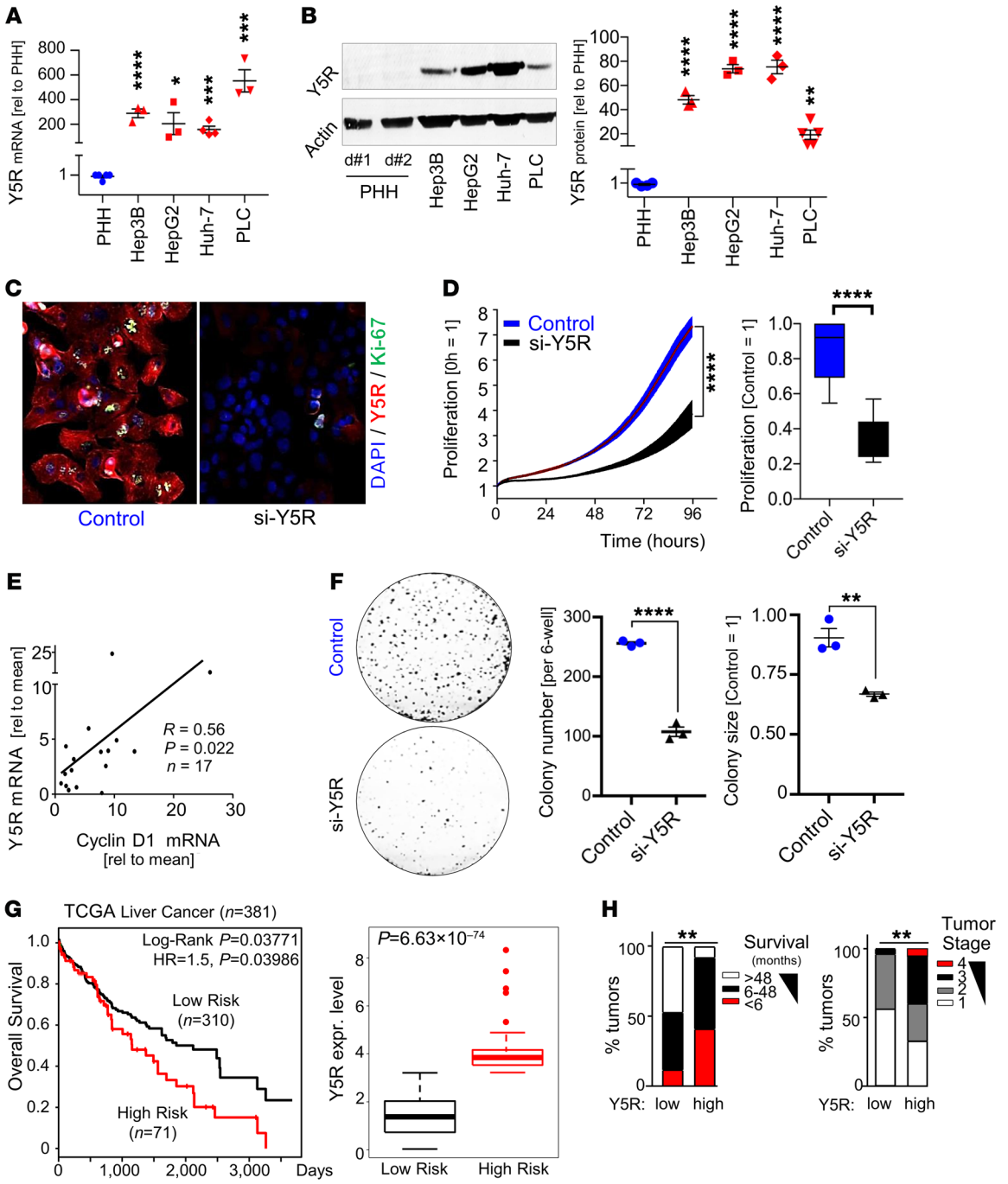

Figure 2. Y5R enhances tumorigenicity of HCC and correlates with poor survival. (**A**) Y5R mRNA levels in primary human hepatocytes (PHH) (n = 5) compared with human HCC cells Hep3B (n = 3), HepG2 (n = 3), Huh-7 (n = 4), and PLC (n = 3). (**B**) Y5R Western blot analysis: representative image (PHHs from 2 donors [d#1, d#2]) and quantification of protein levels (PHHs [n = 4] compared with Hep3B [n = 3], HepG2 [n = 3], Huh-7 [n = 3], PLC [n = 5]). (**C** and **D**) HCC cells transfected with siRNA pools against Y5R (si-Y5R) or a control siRNA pool (Control). (**C**) Coimmunofluorescence (Y5R, Ki-67) images (20-fold original magnification; n = 2). (**D**) Representative proliferation curves and quantification (n = 3) (box-and-whisker plots [min to max]). (**E**) Correlated Y5R and cyclin D1 mRNA (human HCC tissues; n = 17). (**F**) Clonogenicity (colony numbers, sizes, representative images) of PLC cells after RNAi-mediated Y5R knockdown (n = 3). (**G**) SurvExpress analysis of Y5R expression and overall survival (TCGA data; n = 381). Computational stratification (low-risk and high-risk groups) based on prognostic index. (**H** and **I**) Comparison of survival of patients with low (n = 17) and high (n = 39) Y5R expression (**H**) and tumor stages of patients with low (n = 25) and high (n = 92) Y5R expression (**I**) based on IHC analysis of HCC tissue microarray samples. Data are presented as mean ± SEM. Statistical significance was determined by ordinary 1-way ANOVA and Dunnett's multiple-comparisons test (**A** and **B**); 2-tailed, unpaired t test (**D** and **F**); Pearson correlation (**E**); 2-sided Fisher's exact test, Spearman's correlation, and uni- and multivariate analysis (ordinal regression analysis, link function: logit) (**H** and **I**); and log-rank testing and hazard ratio estimates (**G**). *P < 0.05, **P < 0.01, ***P < 0.001, ****P < 0.0001.

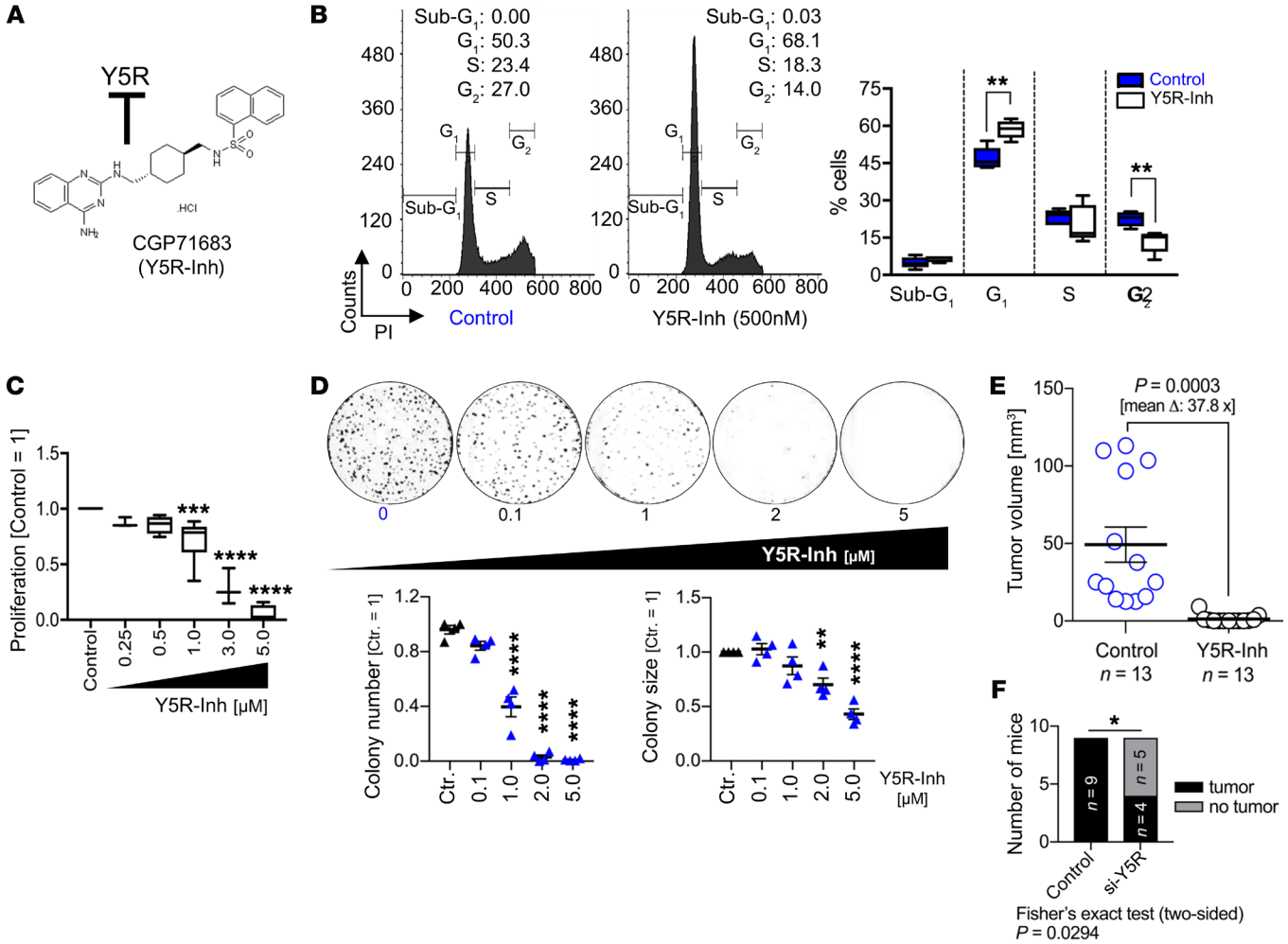

Figure 3. Y5R inhibition impairs tumorigenicity and growth of HCC. (**A**) Chemical formula of the specific, high-affinity Y5R inhibitor CGP71683 (Y5R-Inh). (**B**–**D**) Y5R-Inh–treated as compared with control-treated (i.e., solvent [DMSO]) HCC cells with application of different functional in vitro assays. (**B**) FACS analysis (representative images and quantification) after propidium iodide (PI) staining; quantification of sub-G_1/G_0, G_1, S, and G_2 cell cycle fractions (n = 3) (data are shown as box-and-whisker plots [min to max]). (**C**) Real-time proliferation analysis applying different doses of Y5R-Inh (n = 3) (data are shown as box-and-whisker plots [min to max]). (**D**) Quantification of colony numbers and sizes and representative images with application of clonogenicity assays (n = 4). (**E** and **F**) Murine HCC models of orthotopic syngeneic HCC cell implantation (Hepa129 cells) in C3H mice. (**E**) After HCC cell implantation, mice were randomized into 2 groups and were treated with Y5R-Inh (15 mg/kg body weight, daily i.p. injection for 7 days) or received the solvent only. (**F**) For RNAi-mediated Y5R knockout, transfection of HCC cells was performed for 48 hours before injection into livers, and tumor onset was assessed after 7 days. Data are presented as mean ± SEM. Statistical significance was determined by ordinary 1-way ANOVA together with Dunnett's multiple-comparisons test (**C** and **D**) or 2-tailed, unpaired t test (**B** and **E**), or by 2-sided Fisher's exact test together with Spearman's correlation analysis (**F**). $^*P < 0.05$, $^{**}P < 0.01$, $^{***}P < 0.001$, $^{****}P < 0.0001$.

in HCC patients. In line with this, IHC analysis of human HCC tissues derived from a further patient cohort (tissue microarray) confirmed that high Y5R expression was correlated with poor patient survival (Figure 2H, Supplemental Figure 2H, and Supplemental Table 2) and advanced tumor stages (Figure 2I and Supplemental Table 2).

In summary, these data indicated enhanced Y5R expression in HCC as a promoter of tumor progression and suggested this NPY receptor as a prognostic and potential therapeutic target.

Y5R inhibition impairs tumorigenicity and growth of HCC. The emerging role of the Y5R/NPY axis in obesity (51) has inspired the development of several small molecules for pharmacologic Y5R inhibition. CGP71683 (Y5R-Inh) (Figure 3A) inhibits Y5R with high affinity and selectivity toward other NPY receptors (Supplemental Figure 3A and ref. 52). In vitro, this Y5R inhibitor dose-dependently reduced proliferation and induced G_0/G_1 cell cycle arrest in human HCC cells (Figure 3, B and C, and Supplemental Figure 3, B and C). Clonogenicity assays revealed marked reduction of colony numbers and sizes after treatment with this inhibitor (Figure 3D). These effects of pharmacologic Y5R inhibition on proliferation and clonogenicity were confirmed using 3 further specific small-molecule Y5R inhibitors (Supplemental Figure 3, A and D–F, and refs. 53, 54).

Also in murine HCC cells (including Hepa129, which originate from C3H mice; ref. 55), Y5R was overexpressed in comparison with murine hepatocytes (Supplemental Figure 3, G and H), and pharmacologic Y5R inhibition showed strong antitumorigenic effects in vitro (Supplemental Figure 3I). Hepa129 cells are widely used

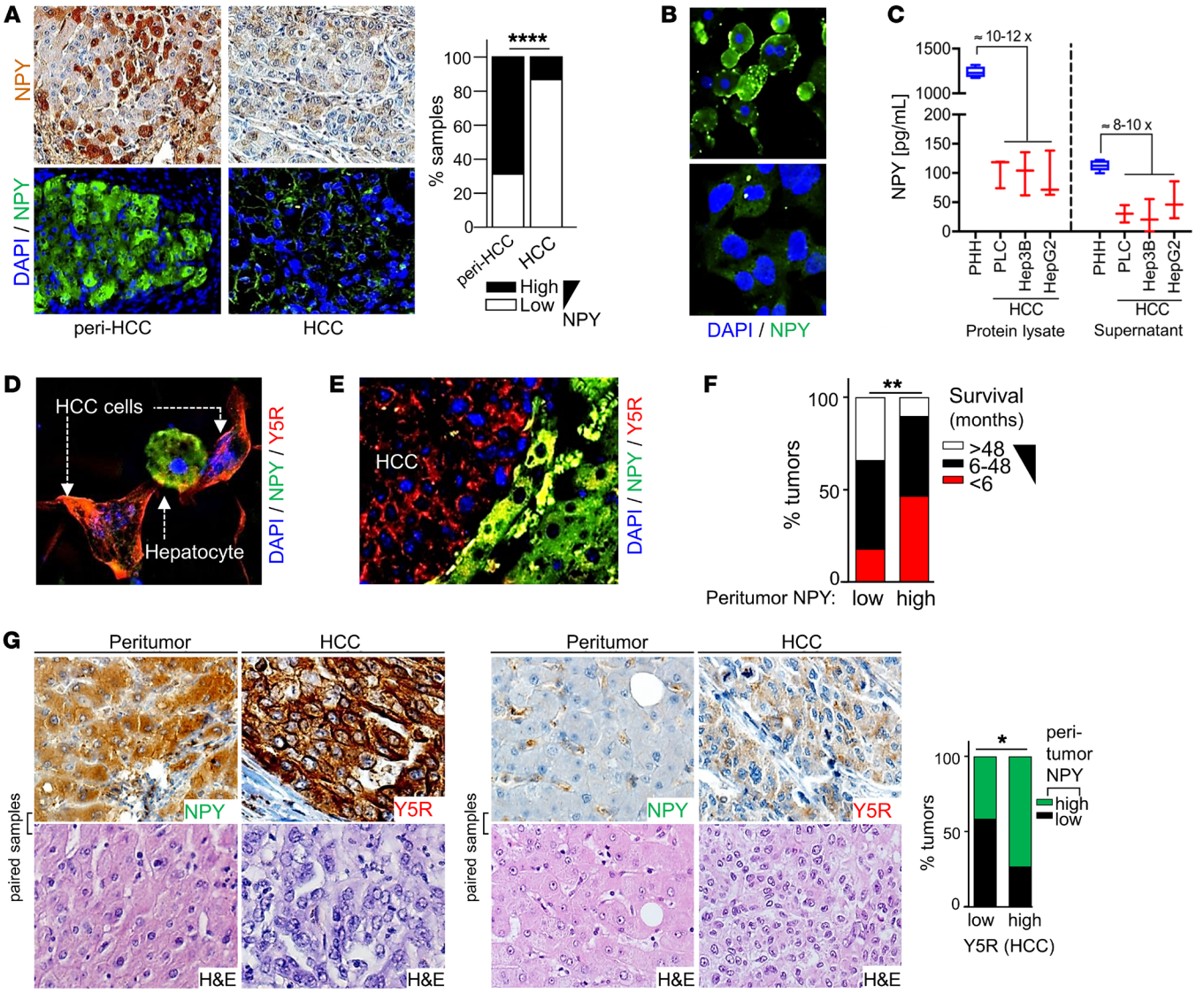

Figure 4. NPY is secreted by peritumorous hepatocytes and correlates with survival and Y5R expression in HCC. (**A** and **B**) Immunohistochemical/immunofluorescence analysis of NPY expression in paired nontumorous (Peri-HCC) and HCC tissues of patients (representative images [20-fold original magnification] and quantification) applying a tissue microarray (n = 231) (**A**) and representative images (40-fold original magnification) displaying primary human hepatocytes (PHH) and HCC cells (Hep3B) (n = 3) (**B**). (**C**) ELISA analysis of NPY expression in protein lysates and in cell culture supernatants of PHHs (n = 4) and HCC cells (PLC [n = 3], Hep3B [n = 3], HepG2 [n = 3]) (data are shown as box-and-whisker plots [min to max]). (**D** and **E**) Coimmunofluorescence staining of NPY and Y5R protein in in vitro cocultures of hepatocytes and HCC cells (n = 2) (40-fold original magnification) (**D**) and the murine orthotopic HCC model (n = 6) (20-fold original magnification) (**E**). (**F**) Comparison of survival of HCC patients with high (n = 31) and low (n = 27) NPY immunoreactivity in peritumorous liver tissue applying a tissue microarray. (**G**) Representative images (40-fold original magnification) and IHC analysis of NPY and Y5R staining of paired peritumorous liver tissues and corresponding HCC tissues applying a human tissue microarray (n = 103). Data are presented as mean ± SEM. Statistical significance was determined by 2-sided Fisher's exact test together with Spearman's correlation analysis (**A**, **F**, and **G**) and uni- and multivariate analysis applying ordinal regression analysis (link function: logit) (**F**). *P < 0.05, **P < 0.01, ****P < 0.0001.

to establish orthotopic HCCs after injection into the liver of syngeneic C3H mice (42, 55). In this model, Y5R was confirmed to be strongly expressed by HCC cells also in vivo (Supplemental Figure 3J), and pharmacologic Y5R inhibition almost completely blocked in vivo tumor formation (Figure 3E and Supplemental Figure 3K). In contrast, no toxic effects of pharmacologic Y5R inhibition were detected in vivo and in vitro (Supplemental Figure 3, L and M). According to pharmacologic inhibition, RNAi-mediated specific Y5R knockdown in Hepa129 cells (Supplemental Figure 3, N and O) confirmed marked reduction of in vivo tumor formation (Figure 3F) and growth (Supplemental Figure 3, P–S). Together, along with RNAi-mediated Y5R suppression, application of pharmacologic small-molecule inhibitors identified this NPY receptor as a critical driver of HCC progression and as an attractive therapeutic target.

NPY is secreted by peritumorous hepatocytes and crosstalks with Y5R in HCC. The strong effects of Y5R in HCC prompted us to further assess the role of its ligand NPY. We had hypothesized so far that serum-derived NPY (Supplemental Figure 2A) is the major inducer of Y5R activation. Unexpectedly, IHC analysis revealed marked NPY expression by hepatocytes surrounding tumor but

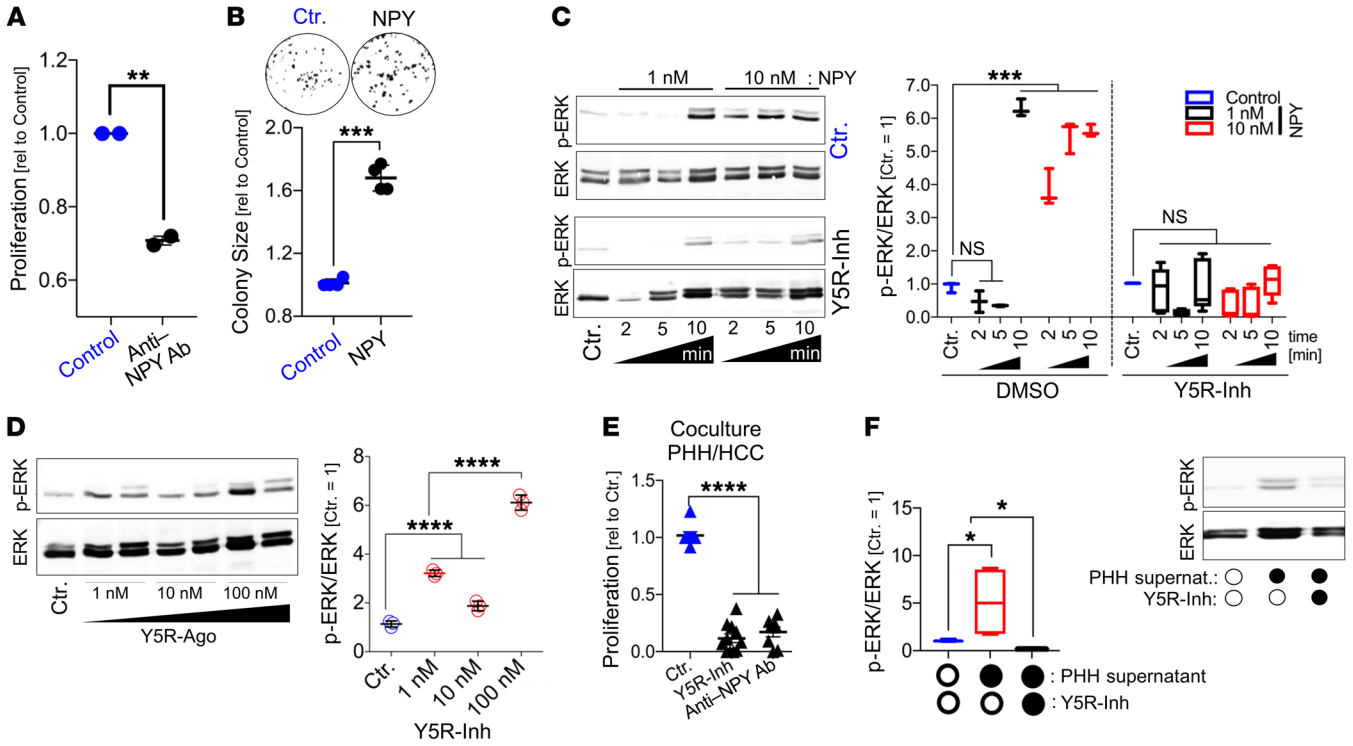

Figure 5. NPY crosstalks with Y5R in HCC. (**A**) Real-time cell proliferation analysis of HCC cells (PLC) in serum-containing (i.e., NPY-containing) culture medium applying an NPY-neutralizing antibody (Anti-NPY Ab) (n = 2; 2 replicates per independent experiment). (**B**) Clonogenicity assay (representative images and quantification of colony sizes) of NPY-treated (500 nM) and control-treated HCC cells (PLC) applying serum-free medium (n = 4). (**C** and **D**) Western blot analysis of phospho-ERK (p-ERK) and ERK levels (representative images and densitometric quantification) of HCC cells (PLC) treated with recombinant NPY with or without combined treatment applying the specific Y5R inhibitor CGP71683 (Y5R-Inh) (n = 3) (**C**) (data are shown as box-and-whisker plots [min to max]), or treated with the specific Y5R agonist (BWX46) (the representative image shows duplicates for Y5R agonist treatment) (n = 3) (**D**). (**E**) Real-time cell proliferation analysis of cocultured HCC cells and PHHs applying the Y5R inhibitor or a neutralizing NPY antibody (Anti-NPY Ab) as compared with control treatment (n = 8). (**F**) Western blot analysis (and representative image) of p-ERK and ERK levels in HCC cells incubated with cell culture supernatant of PHHs (containing NPY as quantified by ELISA) with or without combined treatment applying Y5R-Inh or anti-NPY Ab (n = 3) (data are shown as box-and-whisker plots [min to max]). Data are presented as mean ± SEM. Statistical significance was determined by ordinary 1-way ANOVA together with Dunnett's multiple-comparisons test (**C**, **D**, and **F**), or by 2-tailed, unpaired t test (**A**, **B**, and **E**). $^*P < 0.05$, $^{**}P < 0.01$, $^{***}P < 0.001$, $^{****}P < 0.0001$.

only a weak-staining signal in the majority of tumor cells in human HCC specimens (Figure 4A and Supplemental Figure 4, A–C). In line with this, cultured human hepatocytes expressed and secreted NPY in approximately 10-fold higher amounts compared with HCC cells (Figure 4, B and C). Also applying in vitro cocultures and in the orthotopic HCC mouse model, we observed a striking contrast between pronounced NPY expression in hepatocytes and absence of NPY staining in HCC cells, while the receptor Y5R was exclusively and strongly expressed by HCC cells (Figure 4, D and E, and Supplemental Figure 4, D and E). Importantly, high peritumorous NPY expression in human liver tissues correlated with poor patient survival (Figure 4F and Supplemental Table 4) and was associated with strong Y5R expression by HCC cells (Figure 4G and Supplemental Table 2). These data suggested that next to activation by serum-derived NPY, Y5R could drive liver cancer via direct crosstalk with hepatocyte-derived peritumorous NPY (Supplemental Figure 4F).

Thus, we aimed to functionally verify this potential NPY-Y5R interaction. In the previous functional in vitro experiments, NPY-containing serum had been added to the cell culture medium, and here, applying an NPY-neutralizing antibody significantly reduced the proliferation of HCC cells (Figure 5A). Furthermore, we now applied recombinant NPY to HCC cells in serum-free medium. Previous studies showed that NPY receptors depend on $G_{i/0}$ proteins and RAS signaling, thereby inducing MAPK/ERK and PI3K/AKT pathway activation (56, 57). Here, we found that even high NPY doses (up to 1 μM) did not affect AKT activation in HCC cells (data not shown). However, recombinant NPY induced clonogenicity (Figure 5B) as well as ERK activation in HCC cells with application of low-nanomolar concentrations (Figure 5C). Moreover, NPY-induced ERK activation was completely blocked by cotreatment with a specific Y5R inhibitor (Figure 5C). Likewise, the synthetic high-affinity Y5R-specific agonist BWX46 (Y5R-Ago) (Supplemental Figure 4G) strongly induced ERK activation in HCC cells (Figure 5D). Following an additional approach, we performed coculture experiments with (NPY-producing) hepatocytes and HCC cells (Supplemental Figure 4H). Here, we observed significant inhibition of tumor cell proliferation after treatment with a Y5R inhibitor or with an NPY-neutralizing antibody (Figure 5E). Furthermore, HCC cells treated with hepatocyte-derived (i.e., NPY-containing) supernatant (Supplemental Figure 4I) showed strong Ki-67 expression and ERK activation, which was significantly blocked by Y5R inhibition (Figure 5F and Supplemental Figure 4J).

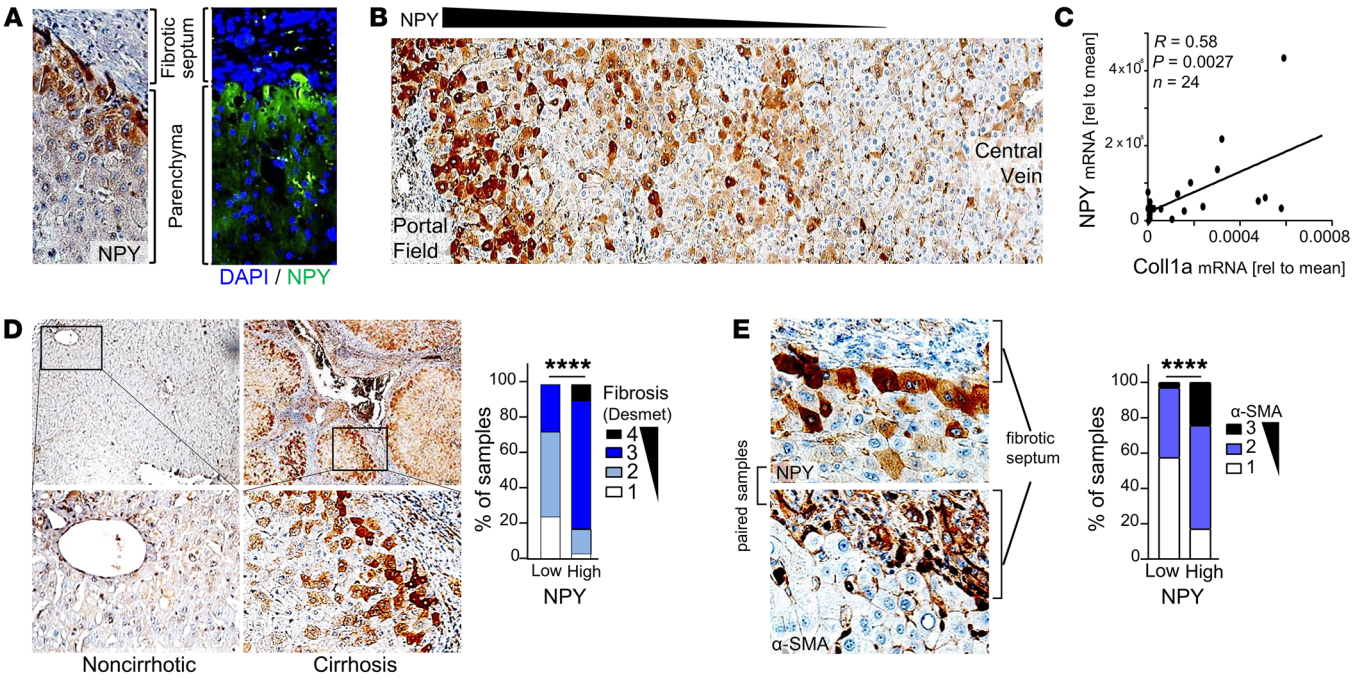

Figure 6. Peritumorous NPY expression by hepatocytes correlates with hepatic fibrosis. (**A** and **B**) Immunohistochemical/immunofluorescence analysis of NPY staining (representative images, 40-fold original magnification in **A**, 20-fold original magnification in **B**) of peritumorous liver tissues applying a tissue microarray (TMA) (n = 231). (**C**) Paired NPY and collagen type I (Coll1a) mRNA expression, by quantitative reverse transcriptase PCR (qRT-PCR) analysis, in human peritumorous liver tissues (n = 24). (**D**) IHC analysis (representative images [10- and 40-fold original magnification, respectively] and quantification) of fibrosis (applying the Desmet score system) in peritumorous liver tissues with high (n = 64) as compared with low (n = 33) NPY expression levels applying a human tissue microarray. (**E**) IHC analysis (representative images and quantification) of α-smooth muscle actin (α-SMA) expression in peritumorous liver tissues with high (n = 58) as compared with low (n = 33) NPY expression levels applying a human TMA; the representative images (40-fold original magnification) display the same loci derived from paired (i.e., serial) tissue sections from 1 patient. Data are presented as mean ± SEM. Statistical significance was determined by Pearson correlation (**C**) or by 2-sided Fisher's exact test together with Spearman's correlation analysis (**D** and **E**). ****$P < 0.0001$.

Together, these data indicated peritumorous hepatocytes as a so-far unknown source of NPY and demonstrated that hepatocyte-derived NPY can drive liver cancer via crosstalk with Y5R on HCC cells.

Peritumorous NPY expression is induced by hepatic fibrosis and TGF-β signaling. Next, we sought insight into the underlying mechanisms that induce peritumorous NPY expression in liver cancer, which usually develops in chronic liver disease (2, 58). Immunohistological analysis of patient-derived tissues revealed that next to peritumorous hepatocytes, the strongest NPY expression was detected around portal fields and fibrotic septa (Figure 6, A and B, and Supplemental Figure 5, A and B).

The activation of hepatic stellate cells (HSCs) is the key event of hepatic fibrosis, with activated HSCs being the major source of extracellular matrix expression and deposition (59, 60). Activation of HSCs is characterized by expression of α-smooth muscle actin (α-SMA) and collagen type I expression (60). Quantitative reverse transcriptase PCR analysis revealed a significant correlation between NPY and collagen expression in peritumorous liver tissues of HCC patients (Figure 6C). Moreover, next to its localization around portal fields and septa, expression of NPY strongly correlated with liver fibrosis/cirrhosis (Figure 6D and Supplemental Table 4). We observed that NPY-positive hepatocytes were closely localized to areas of HSC activation (indicated by, e.g., α-SMA expression) in peritumorous liver tissues (Figure 6E; Supplemental Figure 5, C–E; and Supplemental Table 4). Therefore, we excluded that NPY could also be derived directly from HSCs by applying ELISA and immunofluorescence analysis, revealing that NPY is exclusively expressed by hepatocytes both in vitro and in vivo (Figure 7, A and B). Considering the striking colocalization of HSC activation and NPY-immunopositive hepatocytes, we hypothesized that activated HSCs may induce NPY expression in hepatocytes. In support of this, conditioned cell culture media from activated HSCs induced NPY expression and protein secretion by hepatocytes (Figure 7, C and D).

Activated HSCs are a major cellular source of hepatic TGF-β, which is known as one of the most important mediators of tissue fibrosis (60). Therefore, we used 2 model systems to investigate whether TGF-β could induce NPY expression in hepatocytes: (a) cultured primary human hepatocytes (PHHs) and (b) a hepatoblast-derived liver organoid model representing differentiated hepatocytes in a 3D, in vivo–like system (Supplemental Figure 6A and ref. 61). In both of these models, TGF-β treatment was confirmed to induce a dose-dependent upregulation of mesenchymal markers (Supplemental Figure 6, B and C, and ref. 62). Moreover, in both model systems, TGF-β treatment strongly induced NPY expression in hepatocytes (Figure 7, E and F). In vivo, immunohistological TGF-β staining of human peritumorous liver tissues revealed strong expression in fibrotic septa (Figure 7G). Also, hepatocytes localized close to the fibrotic septa revealed a positive TGF-β immunosignal (Figure 7G). Thus, TGF-β staining strongly resembled the NPY

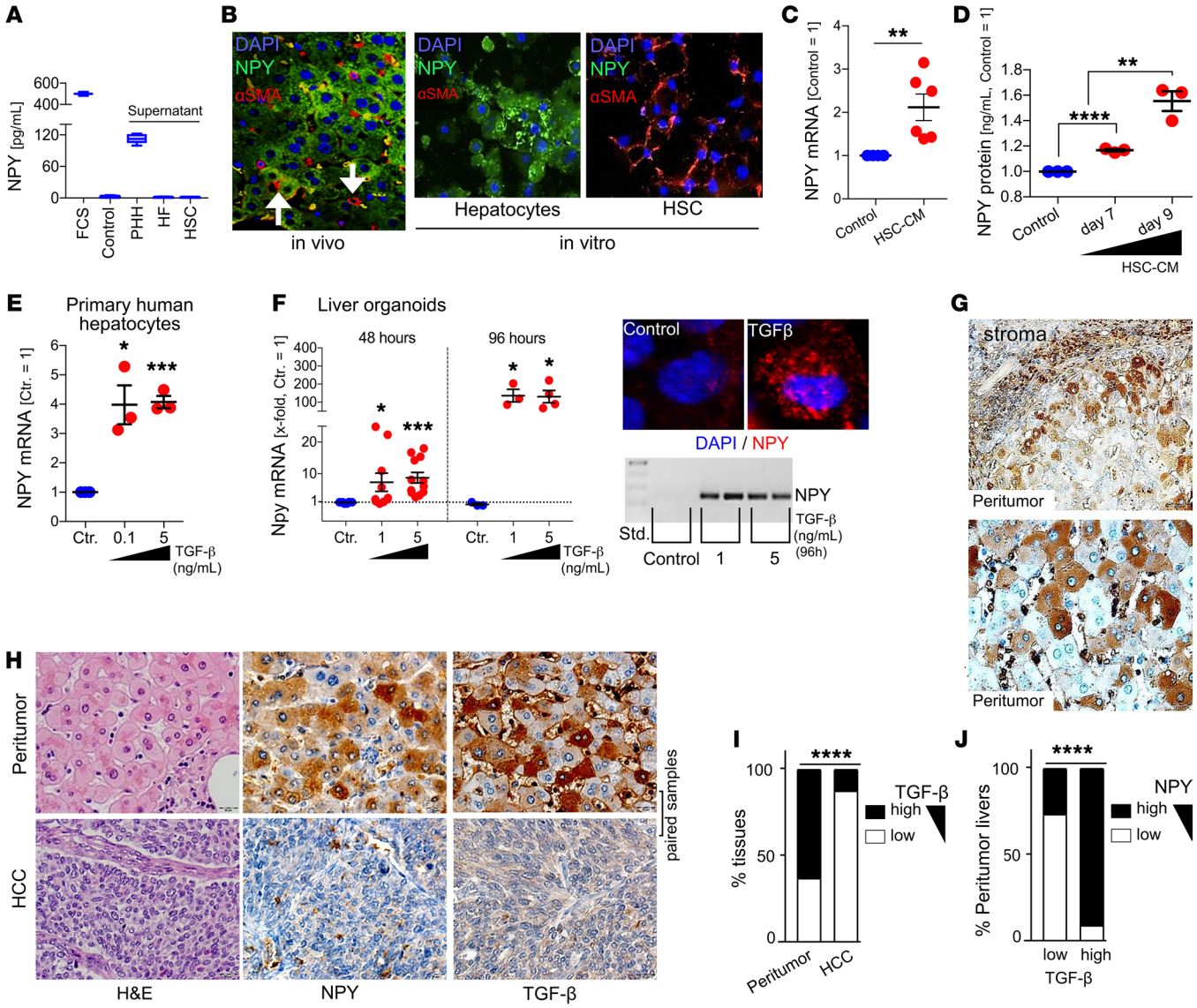

Figure 7. Peritumorous, hepatocyte-derived NPY expression is induced by TGF-β. (**A**) ELISA analysis of NPY protein levels in cell culture medium with FCS (n = 3), serum-free medium (Control; n = 3), and cell culture supernatants of primary human hepatocytes (PHH; n = 6), human fibroblasts (HF; n = 2), and hepatic stellate cells (HSC; n = 3). (**B**) Representative images of (co)immunofluorescence staining (NPY and α-SMA; 20-fold original magnification) of peritumorous liver tissues of C3H mice (left, n = 3) and cultures of PHHs or HSCs (n = 3; right). (**C**) NPY mRNA of PHHs treated or not treated with conditioned culture medium derived from HSCs (HSC-CM; n = 6). (**D**) NPY protein levels in cell culture supernatants treated or not treated with HSC-CM (n = 3). (**E**) NPY mRNA in PHHs treated for 48 hours with different doses of TGF-β (n = 3). (**F**) NPY mRNA in hepatocyte-derived liver organoids treated for 48 hours (n = 10) or 96 hours (n = 4) with TGF-β (left). Representative images of qRT-PCR gel electrophoresis (n = 3) and confocal immunofluorescence (60-fold original magnification; n = 2) (right). (**G**) Representative IHC TGF-β staining of (human) peritumorous liver (40-fold original magnification). (**H**–**J**) IHC analysis of TGF-β and NPY in peritumorous liver and corresponding HCC tissues. (**H**) Representative images (40-fold original magnification). (**I**) Comparison of TGF-β expression in HCC and corresponding peritumorous liver tissues (n = 219). (**J**) Comparison of NPY expression in peritumorous liver tissues with low (n = 38) and high (n = 63) TGF-β expression. Data are presented as mean ± SEM. Statistical significance was determined by ordinary 1-way ANOVA together with Dunnett's multiple-comparisons test (**D**–**F**) or 2-tailed, unpaired t test (**C**), or by 2-sided Fisher's exact test and Spearman's correlation analysis (**I** and **J**). $^*P < 0.05$, $^{**}P < 0.01$, $^{***}P < 0.001$, $^{****}P < 0.0001$.

expression pattern in peritumorous liver tissue. Accordingly, TGF-β expression was higher in peritumorous as compared with HCC tissues (Figure 7, H and I) and significantly correlated with NPY expression in peritumorous liver tissue (Figure 4, H and J, Supplemental Figure 6, D and E, and Supplemental Table 4).

Aiming to address this TGF-β/NPY/Y5R crosstalk functionally, we established a hybrid-organoid model consisting of HCC cells and surrounding hepatocytes (Supplemental Figure 6, F–H). In this system, TGF-β induced (peritumorous) NPY expression by hepatocytes and enhanced HCC growth, which was blocked by Y5R inhibition (Supplemental Figure 6, I and J).

In addition to HSC activation, chronic liver damage is also associated with chronic inflammation (59, 60). Accordingly, we observed that — besides HSC activation — the NPY expression of hepatocytes correlated with the number of infiltrating CD3-positive immune cells (Supplemental Figure 7, A and B, and Supple-

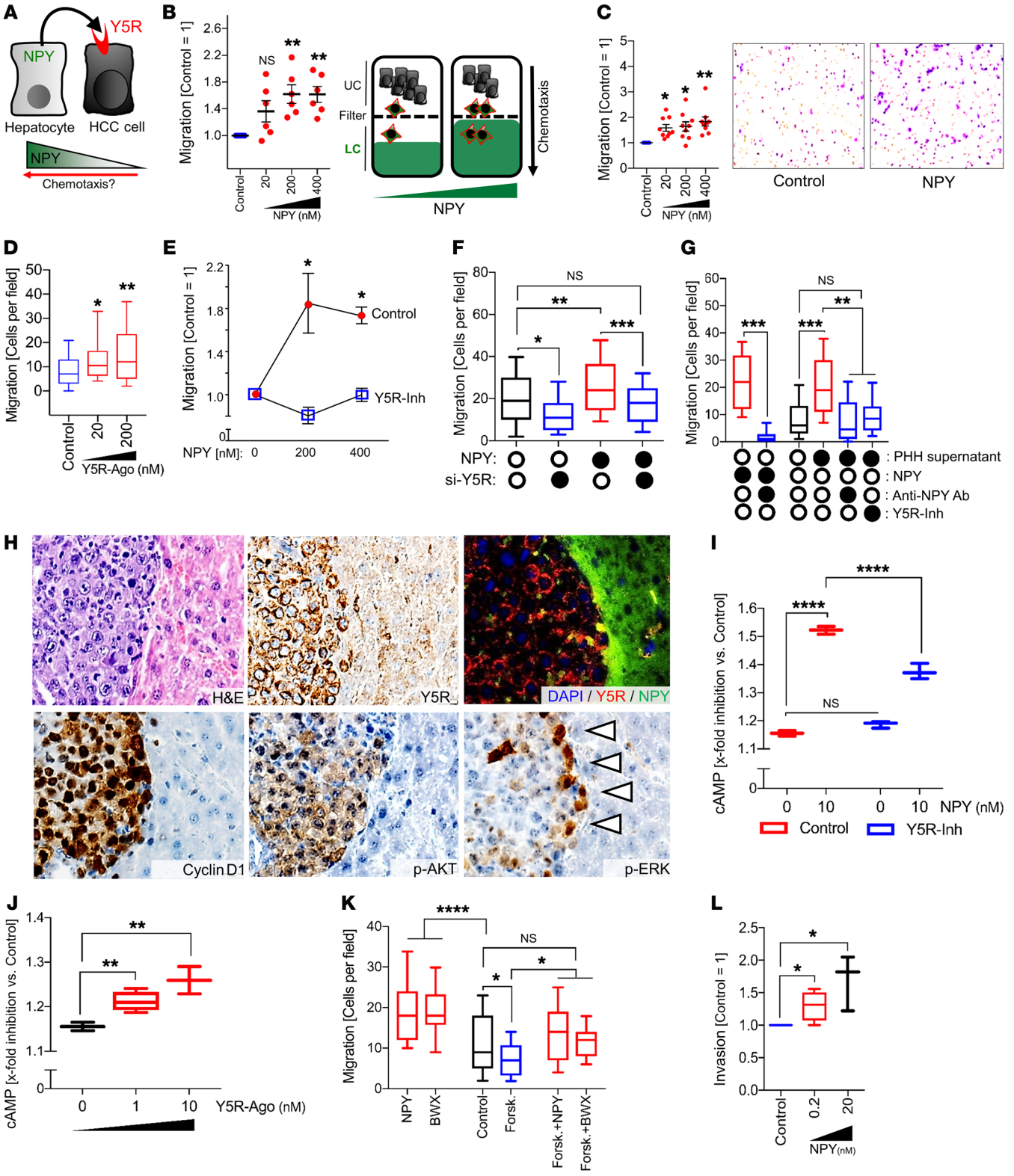
A
Y5R
NPY
Hepatocyte
HCC cell
NPY
Chemotaxis?
B
Migration [Control = 1]
NS
Control
20
200
400
NPY (nM)
UC
Filter
LC
Chemotaxis
NPY
C
Migration [Control = 1]
Control
NPY
D
Migration [Cells per field]
Control
20
200
Y5R-Ago (nM)
E
Migration [Control = 1]
Control
Y5R-Inh
NPY [nM]: 0 200 400
F
Migration [Cells per field]
NS
NPY:
si-Y5R:
G
Migration [Cells per field]
NS
: PHH supernatant
: NPY
: Anti-NPY Ab
: Y5R-Inh
H
H&E
Y5R
DAPI / Y5R / NPY
Cyclin D1
p-AKT
p-ERK
I
cAMP [x-fold inhibition vs. Control]
NS
0 10 0 10 NPY (nM)
Control
Y5R-Inh
J
cAMP [x-fold inhibition vs. Control]
0 1 10 Y5R-Ago (nM)
K
Migration [Cells per field]
NS
NPY
BWX
Control
Forsk.
Forsk.+NPY
Forsk.+BWX
L
Invasion [Control = 1]
Control
0.2
20
NPY(nM)

Figure 8. Hepatocyte-derived NPY mediates chemotaxis via activation of Y5R. (**A**) Cartoon hypothesis that an NPY gradient (downregulation of NPY in HCC cells and NPY expression by peritumorous hepatocytes) impacts chemotaxis of HCC cells via Y5R activation. (**B**–**G**) Real-time cell migration (**B**) and Boyden chamber (**C**–**G**) analysis (upper chamber [UC] and lower chamber [LC]) of chemotaxis of HCC cells toward recombinant NPY (**B** [*n* = 6] and **C** [*n* = 8]), Y5R agonist BWX46 (Y5R-Ago) (*n* = 3) (**D**), and NPY with or without Y5R inhibition by CGP71683 (Y5R-Inh) (*n* = 3) (**E**) or by NPY-mediated and/or siRNA pool–mediated Y5R knockdown (*n* = 3; box-and-whisker plots [min to max]) (**F**). (**G**) NPY or supernatants of primary human hepatocytes (PHH) with or without Y5R-Inh or an NPY-neutralizing antibody (anti-NPY Ab) (*n* = 3; box-and-whisker plots [min to max]). (**H**) Representative IHC (H&E, Y5R, cyclin D1, p-AKT, p-ERK) and coimmunofluorescence (Y5R and NPY) analysis (serial sections) of HCC and peritumorous tissue applying the orthotopic murine HCC model (20-fold original magnification; *n* = 6). Arrowheads: tumor-parenchyma edge. (**I** and **J**) cAMP signaling (analyzed by bioluminescence resonance energy transfer technique) of PLC cells treated with NPY and/or Y5R-Inh (**I**) or different doses of Y5R-Ago (box-and-whisker plots [min to max]; *n* = 3) (**J**). (**K**) Boyden chamber analysis of migration of HCC cells toward NPY or BWX46 with or without cotreatment with the cAMP inducer forskolin (Forsk.) (*n* = 4; box-and-whisker plots [min to max]). (**L**) Boyden chamber analysis of invasion of HCC cells toward NPY in the lower compartment (*n* = 4; box-and-whisker plots [min to max]). Data are presented as mean ± SEM. Statistical significance was determined by ordinary 1-way ANOVA and Dunnett's multiple-comparisons test (**B**–**G** and **I**–**L**). $*P < 0.05$, $**P < 0.01$, $***P < 0.001$, $****P < 0.0001$.

mental Tables 4 and 5). High CD3-positive immune cell infiltration also correlated with enhanced fibrosis and high α-SMA expression in peritumorous liver tissues and was also associated with reduced survival (Supplemental Figure 7B and Supplemental Table 5). We hypothesized that although activated HSCs are considered to be a major cellular source of hepatic TGF-β (60), immune cells further contribute to (NPY-inducing) TGF-β production in the HCC microenvironment. Moreover, further cytokines could affect NPY expression. Screening of several inflammatory cytokines that are known key drivers of chronic liver injury revealed strong correlation of IL-1β and IL-6 with NPY expression in peritumorous liver tissues (Supplemental Figure 7C), while other cytokines, including, e.g., TNF-α (data not shown), showed no correlation with NPY expression. Treatment with recombinant IL-1β caused a moderate but significant increase of NPY expression by hepatocytes (Supplemental Figure 7, D and E). In chronic liver disease, IL-1β is secreted by both activated HSCs (63) and immune cells (64). In contrast to IL-1β, IL-6 treatment did not directly affect NPY expression (Supplemental Figure 7, D and E). However, IL-6 might indirectly promote NPY expression by induction of HSC activation (65).

In summary, we found that hepatic fibrosis and inflammation induced hepatic NPY induction and identified TGF-β as a novel major mediator of (hepatic) NPY expression. Our data further supported that TGF-β–induced NPY derived from (peritumorous) hepatocytes can drive liver cancer via crosstalk with Y5R.

Hepatocyte-derived NPY mediates chemotaxis via activation of Y5R. Besides the observed NPY effects on proliferation and clonogenicity of HCC cells, Y5R has also been described to have chemoattractive characteristics in bone marrow stem cells (66). Therefore, we hypothesized that the NPY gradient induced by (a) downregulation of NPY in HCC cells and (b) marked NPY expression by peritumorous hepatocytes could impact chemotaxis of HCC cells (Figure 8A). According to this hypothesis, high peritumorous NPY expression was shown to correlate with poor patient survival (Figure 4F), and TCGA data analysis revealed that low NPY expression in HCC was associated with high-risk patient cohorts and poor overall survival (Supplemental Figure 8A). When we applied real-time cell migration (xCELLigence; Roche) and Boyden chamber assays, recombinant NPY revealed strong dose-dependent chemoattractive features on HCC cells (Figure 8, B and C, and Supplemental Figure 8, B and C). Similarly, the specific Y5R agonist (BWX46) acted as a strong chemoattractant for HCC cells (Figure 8D). In contrast, small molecule– and siRNA-mediated Y5R inhibition abrogated the chemotactic effects of NPY on HCC cells (Figure 8, E and F, and Supplemental Figure 8D). Also, hepatocyte-derived (i.e., NPY-containing) cell culture supernatants strongly induced chemotaxis of HCC cells (Figure 8G), and this inducing effect was markedly inhibited by cotreatment with a pharmacologic Y5R inhibitor or by application of NPY-neutralizing antibodies (Figure 8G). The molecular link between MAPK/ERK activation and chemotaxis is well known in cancer (67). In line with this, we had found marked induction of ERK signaling by NPY/Y5R crosstalk between hepatocytes and HCC cells (Figure 5, C, D, and F). Moreover, strong ERK activation of HCC cells was exclusively detected at the border of tumors in the orthotopic HCC model (i.e., the site of strong NPY expression by tumor-surrounding hepatocytes) (Figure 8H).

In addition to ERK activation, NPY receptors can inhibit cAMP via activation of G_i proteins (68). In contrast, induction of cAMP signaling was shown to reduce HCC cell migration (69). Therefore, we hypothesized that NPY could also mediate its promigratory/prochemotactic effects via Y5R-mediated cAMP inhibition (in addition to ERK induction). Bioluminescence resonance energy transfer (BRET) analysis revealed significant and dose-dependent inhibition of forskolin-induced cAMP activation in HCC cells by NPY, which was reduced by Y5R inhibition (Figure 8I). BRET analysis also revealed inhibition of forskolin-induced cAMP activation by Y5R agonist treatment (Figure 8J). Functionally, the cAMP inducer forskolin reduced migration of HCC cells, which was (partly) rescued by both NPY and the Y5R agonist BWX46 (Figure 8K). These data suggested that both NPY/Y5R-induced ERK activation and cAMP reduction promote chemotactic migration of HCC cells at tumor-parenchyma borders. Moreover, IHC analysis of human HCC tissues revealed that enhanced peritumoral NPY expression by hepatocytes was significantly associated with stromal invasion (Fisher's exact: $P = 0.001$). In line with this, in addition to migration, NPY also induced chemotactic invasion of HCC cells (Figure 8L).

Together, these findings indicated that in addition to its effect on tumor growth, (peritumorous) NPY crosstalks with Y5R to induce chemotactic migration and might thereby drive invasion and dissemination of HCC cells.

TGF-β induces Y5R expression in HCC cells at sites of stromal invasion. The strong effects of NPY on chemotaxis and invasion prompted us to further explore Y5R expression at sites of stromal invasion. At the invasive front, Y5R was even more strongly expressed in HCC cells than in central tumor areas (Figure 9A). Moreover, IHC analysis revealed that enhanced Y5R expression significantly correlated with stromal invasion in human HCC

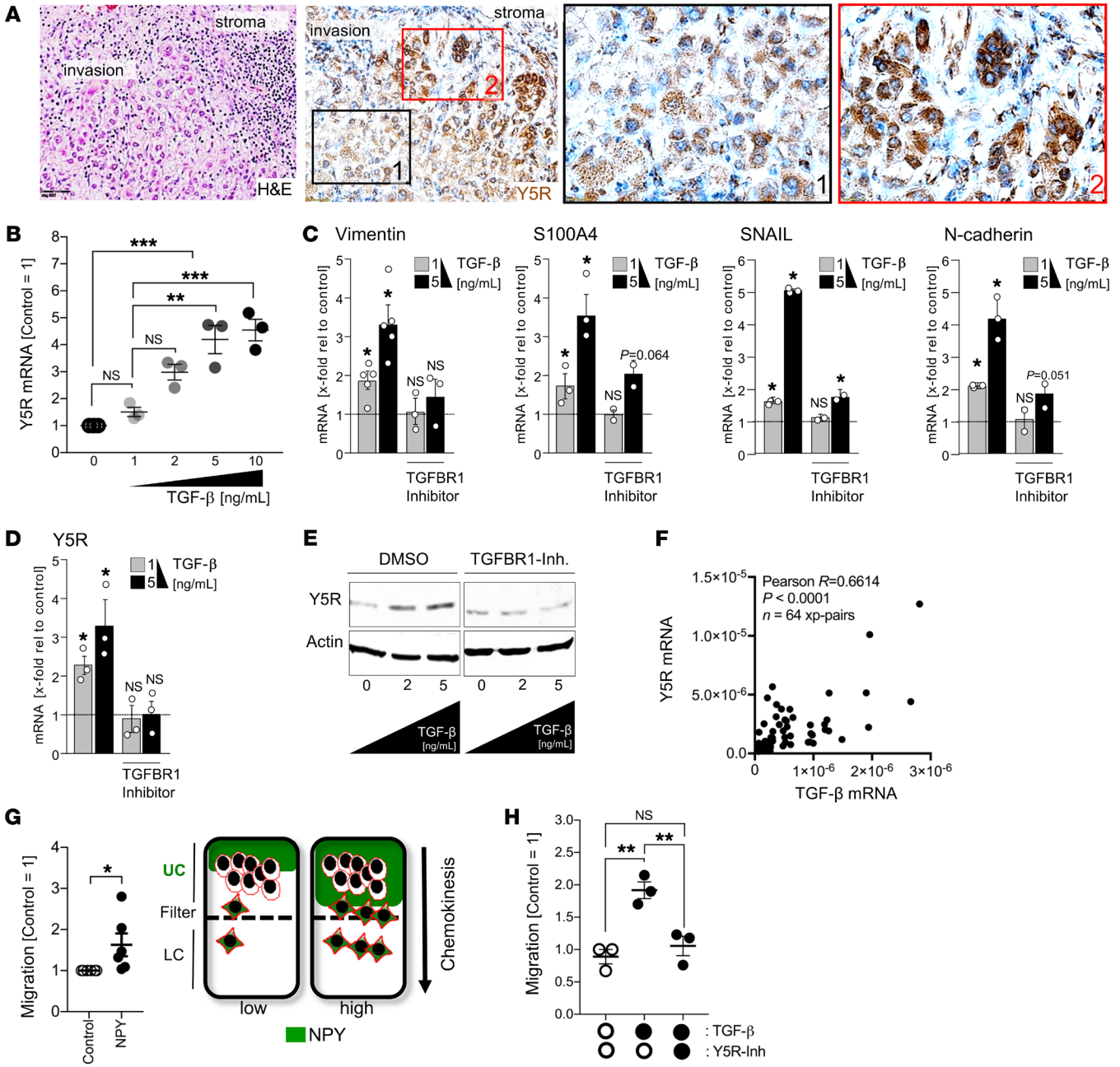

Figure 9. Y5R expression in HCC cells at sites of stromal invasion and TGF-β–mediated effects on Y5R expression in HCC cells. (**A**) Representative images of Y5R (and H&E) immunostaining (10- and 40-fold original magnification, respectively) of human HCC tissues at sites of stromal infiltration (n = 122). (**B**) Y5R mRNA expression levels (qRT-PCR analysis) in HCC cells (PLC) treated with different doses of recombinant TGF-β (n = 3). (**C** and **D**) mRNA expression levels (qRT-PCR analysis) of epithelial-mesenchymal transition (EMT) markers (vimentin, S100A4, SNAIL, and N-cadherin) (**C**) and Y5R (**D**) in HCC cells (PLC) after 96 hours of treatment with recombinant TGF-β with or without cotreatment with the specific TGF-β receptor 1 (TGFBR1) inhibitor galunisertib (10 μM) (n = 3). (**E**) Western blot analysis (representative images, n = 3) of Y5R protein levels in HCC cells after treatment with different doses of TGF-β (96 hours), with or without cotreatment with galunisertib (10 μM). (**F**) Paired Y5R and TGF-β mRNA expression analysis (qRT-PCR analysis, relative to β-actin) in HCC patient tissues (n = 64). (**G**) Real-time cell migration (xCELLigence) analysis of HCC cells (PLC) treated with low-dose recombinant NPY (10 nM) to induce nondirected migration (i.e., chemokinesis) (n = 6). (**H**) Boyden chamber analysis of chemokinesis of HCC cells (PLC) treated or not treated with recombinant TGF-β (5 ng/mL) and/or the specific Y5R inhibitor CGP71683 (Y5R-Inh) (n = 3). Data are presented as mean ± SEM. Statistical significance was determined by ordinary 1-way ANOVA together with Dunnett's multiple-comparisons test (**B**–**D** and **H**), 2-tailed, unpaired t test (**G**), or Pearson correlation (**F**). $^*P < 0.05$, $^{**}P < 0.01$, $^{***}P < 0.001$.

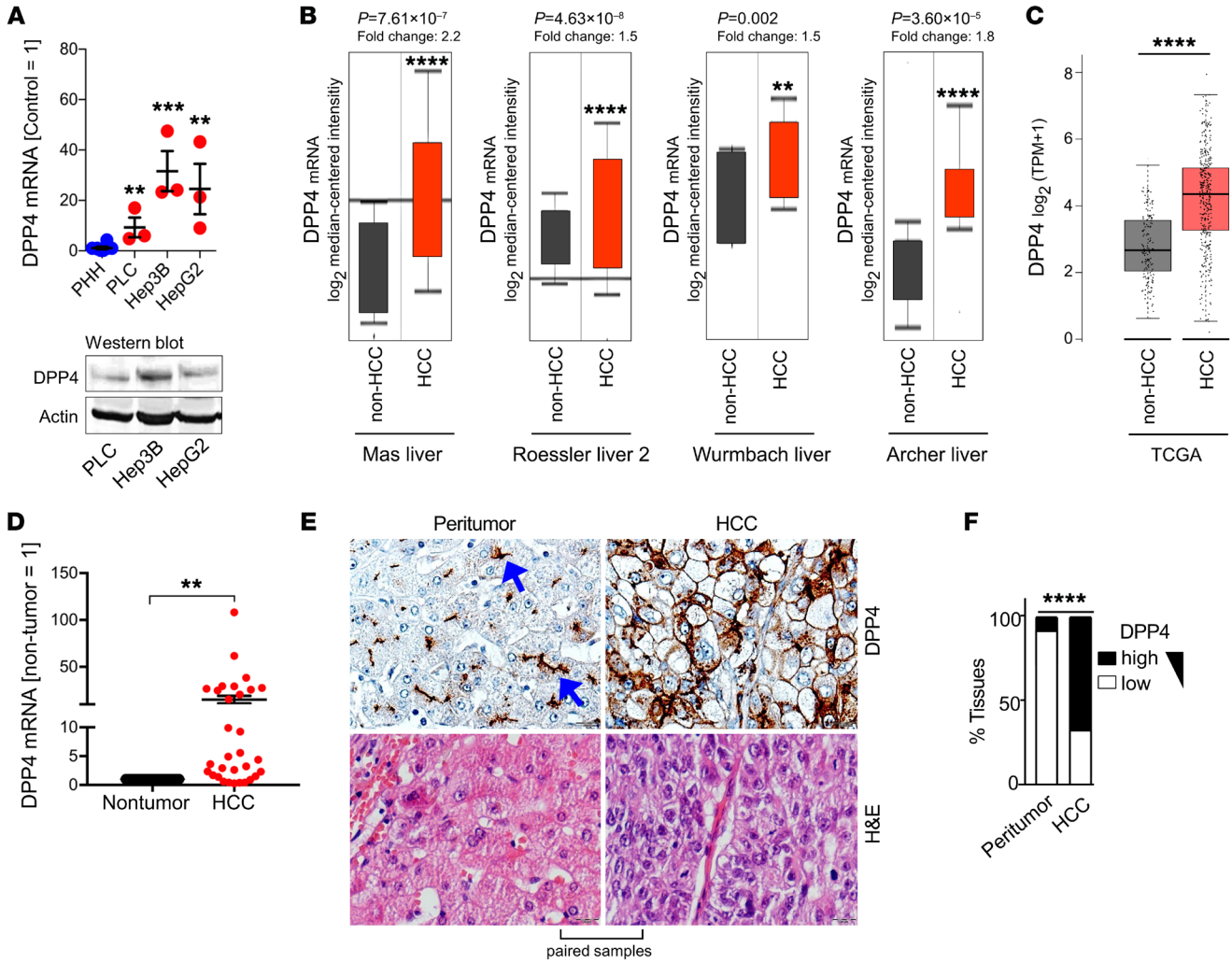

Figure 10. DPP4 is overexpressed in HCC. (**A**) DPP4 mRNA expression (qRT-PCR) in human HCC cell lines (PLC [*n* = 3], Hep3B [*n* = 3], HepG2 [*n* = 3]) compared with primary human hepatocytes (PHH; *n* = 5); below, representative Western blot images depicting DPP4 protein expression in HCC cells (*n* = 2). (**B**) DPP4 RNA expression levels in HCC compared with nontumorous liver tissues (Non-HCC) in different patient data sets from the Oncomine database (Mas liver, non-HCC: *n* = 19, HCC: *n* = 38; Roessler liver 2, non-HCC: *n* = 220, HCC: *n* = 225; Wurmbach liver, non-HCC: *n* = 10, HCC: *n* = 35; Archer liver, non-HCC: *n* = 47, HCC: *n* = 16) (box-and-whisker plots [min to max]). (**C**) Y5R expression in TCGA-derived HCC tissues (*n* = 369) compared with matched nontumorous liver tissues (non-HCC) (*n* = 160) applying the Gene Expression Profiling Interactive Analysis (GEPIA) database. The expression data were first $\log_2$(TPM+1) transformed for differential analysis. (**D**) DPP4 mRNA expression (quantified by qRT-PCR analysis) in paired human HCC and corresponding peritumorous liver tissues (Non-tumor) (*n* = 31). (**E**) Representative IHC DPP4 staining (and H&E staining) (40-fold original magnification) in HCC and corresponding peritumorous liver tissues of the same patients (*n* = 213). Blue arrows show the typical bile canalicular staining pattern of DPP4 in nontumorous hepatocytes. (**F**) Quantification of IHC DPP4 expression in HCC compared with corresponding peritumorous liver tissues of the same patients (*n* = 213). Data are presented as mean ± SEM. Statistical significance was determined by ordinary 1-way ANOVA together with Dunnett's multiple-comparisons test (**A** and **C**), 2-tailed, unpaired *t* test (**B**), or 2-tailed, paired *t* test (**D**), or by 2-sided Fisher's exact test together with Spearman's correlation analysis (**F**). $^{**}P < 0.01$, $^{***}P < 0.001$, $^{****}P < 0.0001$.

(Fisher's exact: $P = 0.041$; Spearman's correlation: $R = 0.24$; $P = 0.007$). In search of the underlying mechanisms, we considered TGF-β, which was found to be highly expressed in the peritumorous regions (Figure 7, G–I) and also in the invasive front together with Y5R (Supplemental Figure 9A). In addition, TGF-β is well known to play a critical role in the orchestration of invasion and the multistep epithelial-mesenchymal transition (EMT) process in different types of cancer, including HCC (70, 71). Treatment of human HCC cells with recombinant TGF-β dose-dependently upregulated the expression of Y5R (Figure 9B) together with established EMT markers (Supplemental Figure 9B and ref. 71).

Preliminary results from phase I/II clinical trials applying the specific TGF-β receptor 1 (TGFBR1) inhibitor LY2157299 (galunisertib) (Supplemental Figure 9C) in HCC patients (ClinicalTrials.gov identifiers: NCT01246986, NCT02906397, NCT02240433, NCT02178358, NCT02423343) have shown improved outcome and changes consistent with a reduction of EMT (72, 73). Here, we confirmed that galunisertib as well as a further specific TGFBR1 inhibitor (SB43152) (Supplemental Figure 9D and ref. 74) inhibited the TGF-β–induced expression of EMT markers in human HCC cells (Figure 9C and Supplemental Figure 9E). Importantly, both specific TGFBR1 inhibitors also completely prevented the TGF-β–

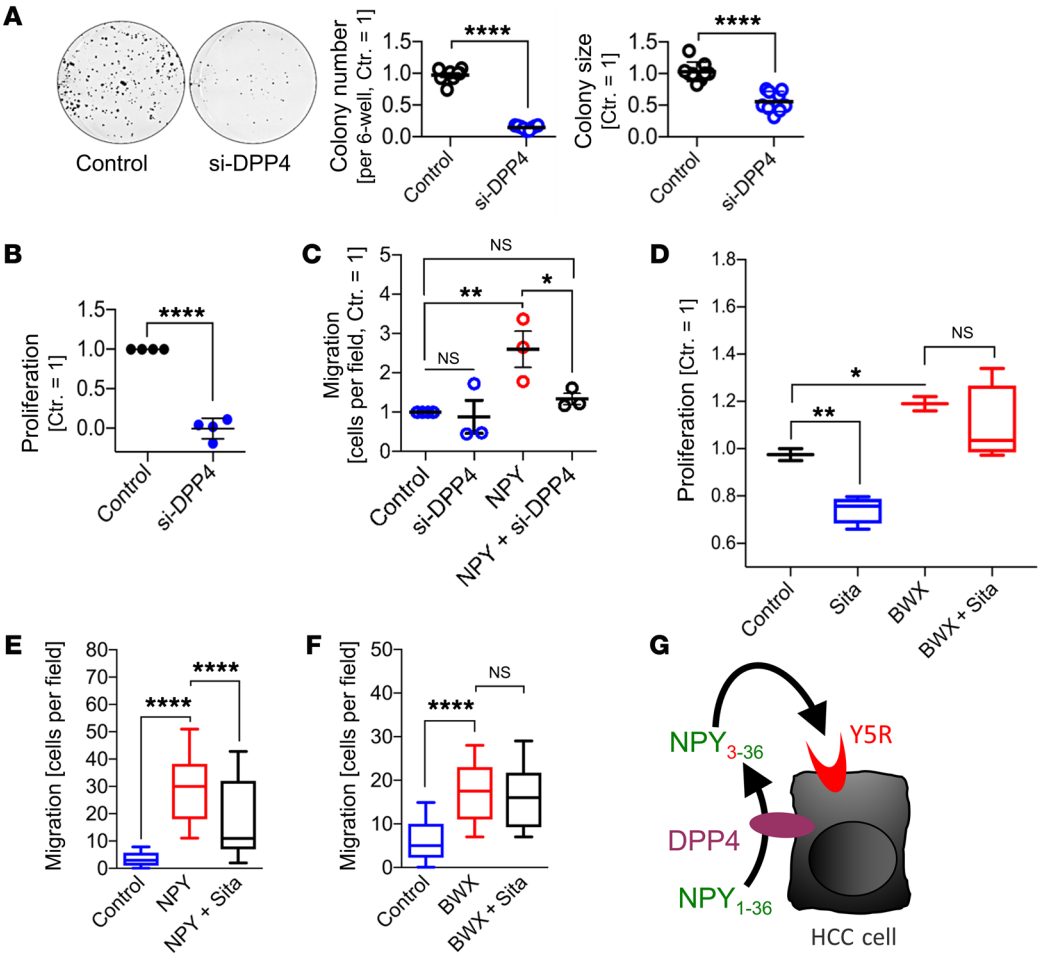

Figure 11. Y5R activation is augmented by DPP4 in HCC. (**A**–**C**) HCC cells were transfected with siRNAs against human DPP4 (si-DPP4) or with control siRNAs (Control). (**A**) Clonogenicity assays (right panels: quantified colony numbers and sizes; left panels: representative images) of HCC cells (Hep3B); data are summarized for Hep3B (n = 6) and PLC (n = 3). (**B**) Real-time cell proliferation analysis (PLC, n = 4). (**C**) Boyden chamber analysis of chemotactic (i.e., directed) migration of HCC cells (PLC) toward control medium or a gradient induced by recombinant NPY (100 nM) with or without combined RNAi-mediated DPP4 knockdown (n = 3). (**D**) Real-time proliferation analysis (xCELLigence) of HCC cells (PLC) using serum-containing (i.e., NPY-containing) culture medium and treatment with sitagliptin (1 μM) with or without cotreatment with the specific Y5R agonist BWX46 (200 nM) (n = 4; box-and-whisker plots [min to max]). (**E** and **F**) Boyden chamber analysis of HCC cells (PLC) migrating toward a gradient induced by recombinant NPY (100 nM) (**E**) or BWX46 (200 nM) (**F**) with or without cotreatment with sitagliptin (1 μM) (n = 4; box-and-whisker plots [min to max]). (**G**) Summary and cartoon depicting the hypothesis that DPP4-mediated NPY conversion to (more Y5R-specific) truncated NPY_{3-36} results in augmented Y5R activation. Data are presented as mean ± SEM. Statistical significance was determined by ordinary 1-way ANOVA together with Dunnett's multiple-comparisons test (**C**–**F**) or 2-tailed, unpaired t test (**A** and **B**). $^*P < 0.05$, $^{**}P < 0.01$, $^{****}P < 0.0001$.

mediated upregulation of Y5R in HCC cells as well as in HCC-HSC cocultures (Figure 9, D and E, and Supplemental Figure 9, F and G), indicating that TGF-β effects on Y5R expression of HCC cells are mediated via canonical and not via noncanonical TGF-β signaling. Moreover, Y5R mRNA levels strongly correlated with TGF-β expression in HCC patient–derived tissue samples (Figure 9F), further supporting the impact of TGF-β/TGFBR1 signaling on Y5R expression of HCC cells.

Conversely, treatment with recombinant NPY or the specific Y5R agonist induced SNAIL expression in HCC cells (Supplemental Figure 9H). Moreover, we found that incubation with NPY or the specific Y5R agonist also induced chemokinetic (i.e., nondirected) migration of HCC cells via Y5R activation (Figure 9G and Supplemental Figure 9I) in addition to the above-described chemoattractive effects. Therefore, considering the strong local coexpression of TGF-β, Y5R, and NPY at sites of stromal invasion, TGF-β might promote HCC cell dissemination (75) by activation of the Y5R/NPY axis. Accordingly, Boyden chamber assays confirmed that pretreatment with TGF-β induced the migratory activity of HCC cells, which was completely blocked by Y5R inhibition (Figure 9H). Considering these findings, we hypothesized that TGF-β might also (co)regulate the age-dependent Y5R expression that we had observed in the experimental C3H mouse model and in liver tissues of HCC patients (Figure 1 and Supplemental Figure 1). However, we found that in neither C3H mice nor human tissues did TGF-β correlate (positively) with age or with age-associated Y5R expression (Supplemental Figure 9, J–L).

In summary, these findings indicated that TGF-β is not only a so-far unknown inducer of (hepatic) NPY expression but also promotes the expression of the NPY receptor Y5R in cancer cells at

the site of stromal invasion via activation of the canonical TGF-β/TGFBR1/2-dependent pathway. Moreover, our data suggest that at least part of the TGF-β/TGFBR1/2 signaling–mediated effect on EMT and stromal invasion is mediated via Y5R activation.

Y5R activation is augmented by dipeptidylpeptidase 4 overexpression in HCC. In contrast to Y5R, the Y1 and Y2 receptor subtypes (Y1R and Y2R) were not regulated by TGF-β signaling (data not shown). Furthermore, Y1R and Y2R were not overexpressed in murine and human HCC and revealed no oncogenic functions in liver cancer (Supplemental Figure 10, A–S). Therefore, Y5R was identified as the only NPY receptor that serves as a potent candidate oncogenic target in liver cancer.

The so-called NPY-converting enzyme dipeptidylpeptidase 4 (DPP4) is a cell surface enzyme that has also a soluble form. DPP4 terminates the Y1R activity of NPY by cleaving Tyr_1 and Pro_2 from NPY_{1-36} to form NPY_{3-36}, which more specifically activates Y5R (76, 77). Just recently, it has been described that hepatocytes secrete DPP4 and thereby promote insulin resistance and adipose tissue inflammation in obese patients (78). We therefore asked whether DPP4-induced NPY conversion to Y5R-specific NPY_{3-36} might contribute to Y5R-mediated HCC progression. We found that DPP4 expression levels were markedly increased in human HCC cell lines compared with poor expression in hepatocytes (Figure 10A). Also applying several patient-derived data sets, including TCGA data, as well as in our patient-derived samples, we detected a strong overexpression of DPP4 levels in HCC tissues as compared with (corresponding) nontumorous liver tissue (Figure 10, B–D). In hepatocytes, DPP4 was described to be mainly localized on the bile canalicular surface (79). We detected a similar distribution of DPP4 immunoreactivity in peritumorous patient tissues and strong expression in most HCC tissues. In some tumor tissues (but not in nontumorous liver tissues), the HCC cells revealed strong DPP4 expression on the entire cell membrane, which could be explained by a loss of polarity of cancer cells (Figure 10E and Supplemental Figure 11A). Confirming in vitro, in silico, and in vivo analysis of DPP4 (mRNA) expression levels, DPP4 immunoreactivity revealed strongly enhanced protein expression in most HCC tissues as compared with nontumorous liver tissue (Figure 10, E and F, and Supplemental Figure 11A). In line with these data, potential interaction of DPP4 with the NPY/Y5R axis in HCC was supported by strong correlation of DPP4 and Y5R expression levels in HCC patient–derived tissue samples (Supplemental Figure 11, A and B) as well as by co-upregulation of DPP4 and Y5R mRNA expression in HCC compared with corresponding nontumorous tissues (Supplemental Figure 11C). High DPP4 protein expression in HCC cells also correlated with peritumorous NPY expression (Supplemental Table 6). Analysis of a TCGA-derived HCC patient cohort revealed that high expression of DPP4 by itself showed a (nonsignificant) trend toward correlation with poor survival (Supplemental Figure 11D). However, combined elevated tumorous DPP4 and Y5R expression together with enhanced peritumorous NPY expression was significantly correlated with poor HCC patient survival (Supplemental Figure 11E). Together, these data supported that NPY derived from peritumorous hepatocytes could be locally converted by DPP4 to enhance Y5R activation and receptor-subtype specificity to drive liver cancer.

Based on these findings and hypotheses, we aimed to functionally analyze the impact of DPP4 inhibition on the pro-tumorigenic action of Y5R in HCC cells. Therefore, RNAi-mediated specific knockdown of DPP4 was performed in HCC cells (Supplemental Figure 11F). Applying serum-supplemented (i.e., NPY-containing) culture media, subsequent analysis revealed strong reduction of both clonogenicity (Figure 11A) and proliferation (Figure 11B) of HCC cells after DPP4 knockdown. In contrast, Boyden chamber analysis of migration applying serum-free (i.e., without NPY) culture media as a chemoattractant showed no effect of DPP4 knockout, while enhanced chemotaxis mediated by recombinant NPY was prevented by combined DPP4 knockout (Figure 11C).

Besides NPY, DPP4 cleaves glucagon-like peptide 1 (GLP-1), which is strongly involved in glucose metabolism. Therefore, orally administered specific DPP4 inhibitors like sitagliptin (Supplemental Figure 11G) have become clinically successful standard therapeutic agents for type 2 diabetes (80). Here, we used sitagliptin to confirm the effects of DPP4 knockout on NPY-mediated Y5R activation as well as to analyze the use of gliptins as a potential pharmacologic application to target the DPP4/NPY/Y5R axis in HCC. Sitagliptin dose-dependently reduced proliferation of HCC cells in serum-containing (i.e., NPY-containing) culture medium (Supplemental Figure 11H), and this inhibitory effect was rescued by the specific Y5R agonist BWX46 (Figure 11D). Moreover, NPY-induced chemotaxis of HCC cells was significantly reduced by sitagliptin (Figure 11E). In contrast, sitagliptin did not affect chemotaxis induction by the specific Y5R agonist (BWX46), which has no DPP4 cleavage site (Figure 11F).

Together, these data indicated that Y5R stimulation in HCC is promoted by DPP4-induced NPY conversion to truncated NPY_{3-36}, which terminates Y1R specificity and augments Y5R specificity (Figure 11G). Our findings suggest DPP4 inhibition using clinically established drugs as a further promising therapeutic strategy to target the newly identified NPY/Y5R axis in HCC.

Discussion

Numerous studies suggested that the NPY system might play a critical role in aging and lifespan as well as in further cancer-related hallmarks (17, 19–24, 51). Hypothalamic NPY levels decrease in aged animals (18), and a reduced cerebral NPY production could contribute to altered reproductive function and food intake in aged subjects (81). In contrast, activation of the NPY system was shown in several human disorders, including chronic liver disease (25, 26, 82) as well as hepatic glucose (29) and lipid (30) metabolism, but its potential role in liver cancer was unknown.

In this study, we found that the expression of the NPY5 receptor (Y5R) in peritumorous liver tissues increased with age both in a mouse model and in patients. This might reflect a compensatory upregulation of Y5R due to low systemic levels of its ligand NPY in aged humans (83). Furthermore, it might result from age-related alterations of methylation of the Y5R promoter. After malignant transformation, HCC cells take advantage of a further upregulation of Y5R expression, which is induced by microenvironment-derived factors including TGF-β. Moreover, in addition to systemic serum-derived NPY, Y5R gets activated via crosstalk with local NPY derived from peritumorous hepatocytes.

Deciphering the underlying mechanisms of peritumorous NPY secretion by hepatocytes, we revealed that hepatic fibrosis contributes to NPY induction and identified TGF-β/TGFBR1 signaling as a major novel mediator of NPY expression by hepatocytes. Strikingly, TGF-β is considered to be a potent modulator of fibrosis and HCC development (84–86).

Conversely, we found that non-Y5 NPY receptors (Y1R and Y2R) were downregulated and did not have tumor-promoting functions in HCC. Actually, Y1R even revealed suppressive effects on tumor cell migration, which is in accordance with the only study that investigated the potential function of an NPY receptor in liver cancer so far (87). In line with our findings, Lv et al. observed that Y1R is downregulated in HCC and that forced overexpression of Y1R mediates tumor suppressor functions in HCC cells (87). In contrast to this single study on Y1R function, the potential roles of NPY, Y2R, and Y5R in HCC had been entirely unknown. Here we show, for the first time to our knowledge, that the NPY/Y5R axis mediates proliferation, stemness-associated properties, chemotactic migration, and invasion in liver cancer. A previous study found that stimulation of Y1R could induce TGF-β secretion by macrophages and thereby affected neuroprotection and hematopoietic stem cell survival in the bone marrow (88). However, to the best of our knowledge, a (converse) regulation of the NPY system by TGF-β has not yet been described.

Here, we revealed that NPY expression in hepatocytes and Y5R expression in HCC cells are regulated via TGF-β/TGFBR1 signaling. Furthermore, our study indicated that TGF-β–mediated effects on HCC tumorigenicity are at least in part mediated by Y5R activation. Besides canonical (TGFBR1-dependent) signaling, TGF-β can also activate Smad1/5/8 (i.e., BMP-associated) pathways through activin receptor–like kinase 1 (ALK1) together with TGFBR2 (89). Indeed, ALK1-dependent signaling represents a potential alternative mechanism of TGF-β signaling in HCC, and the ALK1 inhibitor dalantercept is currently investigated in clinical trials in HCC patients (90). However, our study provides mechanistic evidence that the effects of TGF-β signaling on the NPY/Y5R axis in HCC are mediated via the canonical, TGFBR1-related pathway. Therefore, pharmacologic inhibition of the TGF-β/TGFBR1 axis might represent a potential strategy to target the NPY/Y5R axis in HCC.

We further found that the NPY-converting enzyme DPP4 is upregulated in HCC and augments Y5R function. DPP4 was recently linked to aging and has been shown to be involved in age-dependent dysfunction of bone and hematopoietic regeneration (91). Moreover, a recent study reported that hepatocyte-secreted DPP4 in obesity promotes adipose inflammation and insulin resistance (78), further promoting the value of clinically established DPP4 inhibition for the treatment of (different components of) the metabolic syndrome and its complications. Here, we found that Y5R stimulation in HCC is promoted by DPP4-induced NPY conversion, which terminates Y1R specificity and augments Y5R specificity. Thus, our study suggests that in addition to direct targeting of Y5R or the TGF-β/TGFBR1/NPY/Y5R axis, DPP4 inhibition might represent a further attractive therapeutic strategy for controlling liver cancer.

Regarding potential further therapeutic applications, we revealed that the NPY/Y5R axis activates MAPK/ERK signaling. Therefore, future studies could examine whether Y5R might contribute to efficacy and/or therapy resistance of current first-line therapeutic options for advanced HCC (e.g., sorafenib) that are known to target the RAF/ERK axis.

In summary, targeting the TGF-β/NPY/DPP4/Y5R axis could represent a novel therapeutic avenue in HCC and also other types of cancer.

Methods

Animal models. Eighteen-month-old male C3H/HeN mice were used as a model system of age-related spontaneous hepatocarcinogenesis as previously described (32–38). A murine orthotopic HCC allograft model (42) was used to analyze the therapeutic effect of the specific small-molecule Y5R inhibitor CGP71683 (52) as well as the effect of RNAi-mediated Y5R knockout. Animals were obtained from Charles River Laboratories and housed under specific pathogen–free and controlled conditions.

Human cells and tissues. Pairs of human HCC tissues and corresponding nontumorous liver tissues were obtained from patients after partial hepatectomy. Informed consent was obtained through the Human Tissue and Cell Research (HTCR) Foundation (92). The samples were immediately snap-frozen and stored at –80°C.

The tissue microarray (Supplemental Tables 1–8) consisted of paired HCC and corresponding non-neoplastic liver tissues obtained from HCC patients undergoing surgical resection and was previously described (42).

Statistics. Results were expressed as mean ± SEM. Comparison between groups was made using the 2-tailed Student's *t* test or 1-way ANOVA together with Dunnett's multiple-comparisons test if appropriate. Spearman and Pearson correlation coefficients, respectively, were used for correlation analysis. Analysis of tissue microarrays was performed using Fisher's exact test, Spearman correlation analysis, and uni- and multivariate analysis applying the SPSS ordinal regression procedure (Polytomous Universal Model [PLUM]; link function: logit) (Supplemental Table 9). In silico survival analysis was performed computationally applying log-rank testing and hazard ratio estimates. A P value less than 0.05 was considered significant. The level of significance is depicted in figures as $^{*}P < 0.05$, $^{**}P < 0.01$, $^{***}P < 0.001$, and $^{****}P < 0.0001$. The number of experiments is given in the figure legends. Calculations were performed using Prism software (GraphPad Software Inc.) and SPSS (SPSS Statistics 23, IBM Corp.).

Study approval. The animal studies were approved by the Committee for Animal Health and Care of the local government (Regierung von Mittelfranken, Bavaria, Germany) (RUF-55.2.2-2532-2-566-11), and conformed to international guidelines on the ethical use of animals.

Patients signed an informed consent in accordance with the Helsinki Declaration before being enrolled in the study. The Biobank at the Hospital of the Ludwig-Maximilian University of Munich (HTCR) is under the administration of the nonprofit state-controlled HTCR Foundation, following ethical approval (LMU Munich, no. 25-12).

More detailed procedures can be found in Supplemental Methods.

Author contributions

PD, AKB, and CH conceived the project, analyzed the data, and wrote the paper. PD, LW, VF, TS, MDM, AS, CG, TI, and AT designed and performed the experiments. AEK, WET, JT, AH, MFN, SVH, AKB, and CH provided material and contributed to data analysis and manuscript creation.

Acknowledgments

This work was supported by grants from the German Research Association (DFG) (Research Training Group RTG 1962/1 and FOR 2127 to PD, AKB, and CH), German Cancer Aid (Deutsche Krebshilfe; to PD and AKB), the Bavarian Research Network for Molecular Biosystems (BioSysNet; to AKB), the Else-Kröner-Fresenius Stiftung (to PD), and the Interdisciplinary Center for Clinical Research (IZKF) Erlangen (to PD, AKB, and CH). We thank Reiner Wiest (Inselspital, Bern, Switzerland) for valuable suggestions and critical discussion of the manuscript. We thank Annette Serwotka, Darleen Schönwälder, Sabrina Freitag, Manuel Munz, and Rudolph Jung for excellent technical assistance. We acknowledge the Human Tissue and Cell Research (HTCR) Foundation (Regensburg, Germany) for making human tissue available for research, as well as Hepacult GmbH (Planegg/Martinsried, Germany) for providing primary human hepatocytes for in vitro studies. We appreciate the provision of suitable samples by the Biobank under the administration of HTCR at the Hospital of the Ludwig-Maximilian University of Munich based on extensive data and sample analysis.

Address correspondence to: Claus Hellerbrand, Institute of Biochemistry, Emil-Fischer-Zentrum, Friedrich-Alexander University Erlangen-Nürnberg, Fahrstraße 17, 91054 Erlangen, Germany. Phone: 49.9131.85.24644; Email: claus.hellerbrand@fau.de. Or to: Peter Dietrich, Department of Medicine 1, University Hospital Erlangen, Ulmenweg 18, 91054 Erlangen, Germany. Phone: 49.9131.85.45221; Email: peter.dietrich@fau.de.

1. Yang JD, Hainaut P, Gores GJ, Amadou A, Plymoth A, Roberts LR. A global view of hepatocellular carcinoma: trends, risk, prevention and management. *Nat Rev Gastroenterol Hepatol*. 2019;16(10):589–604.
2. Dietrich P, Hellerbrand C. Non-alcoholic fatty liver disease, obesity and the metabolic syndrome. *Best Pract Res Clin Gastroenterol*. 2014;28(4):637–653.
3. El-Serag HB, Rudolph KL. Hepatocellular carcinoma: epidemiology and molecular carcinogenesis. *Gastroenterology*. 2007;132(7):2557–2576.
4. de Magalhães JP. How ageing processes influence cancer. *Nat Rev Cancer*. 2013;13(5):357–365.
5. Peto J. Cancer epidemiology in the last century and the next decade. *Nature*. 2001;411(6835):390–395.
6. Hanahan D, Weinberg RA. Hallmarks of cancer: the next generation. *Cell*. 2011;144(5):646–674.
7. López-Otín C, Blasco MA, Partridge L, Serrano M, Kroemer G. The hallmarks of aging. *Cell*. 2013;153(6):1194–1217.
8. Ziegler MG, Lake CR, Kopin IJ. Plasma noradrenaline increases with age. *Nature*. 1976;261(5558):333–335.
9. Seals DR, Esler MD. Human ageing and the sympathoadrenal system. *J Physiol (Lond)*. 2000;528(pt 3):407–417.
10. Renz BW, et al. β2 Adrenergic-neurotrophin feedforward loop promotes pancreatic cancer. *Cancer Cell*. 2018;33(1):75–90.e7.
11. Thaker PH, et al. Chronic stress promotes tumor growth and angiogenesis in a mouse model of ovarian carcinoma. *Nat Med*. 2006;12(8):939–944.
12. Magnon C, et al. Autonomic nerve development contributes to prostate cancer progression. *Science*. 2013;341(6142):1236361.
13. Li J, et al. Monoamine oxidase A suppresses hepatocellular carcinoma metastasis by inhibiting the adrenergic system and its transactivation of EGFR signaling. *J Hepatol*. 2014;60(6):1225–1234.
14. Hirsch D, Zukowska Z. NPY and stress 30 years later: the peripheral view. *Cell Mol Neurobiol*. 2012;32(5):645–659.
15. Clarke J, Benjamin N, Larkin S, Webb D, Maseri A, Davies G. Interaction of neuropeptide Y and the sympathetic nervous system in vascular control in man. *Circulation*. 1991;83(3):774–777.
16. Yi M, et al. A promising therapeutic target for metabolic diseases: neuropeptide Y receptors in humans. *Cell Physiol Biochem*. 2018;45(1):88–107.
17. Botelho M, Cavadas C. Neuropeptide Y: an anti-aging player? *Trends Neurosci*. 2015;38(11):701–711.
18. Aveleira CA, et al. Neuropeptide Y stimulates autophagy in hypothalamic neurons. *Proc Natl Acad Sci U S A*. 2015;112(13):E1642–E1651.
19. Yang Y, Atasoy D, Su HH, Sternson SM. Hunger states switch a flip-flop memory circuit via a synaptic AMPK-dependent positive feedback loop. *Cell*. 2011;146(6):992–1003.
20. Marsh DJ, Hollopeter G, Kafer KE, Palmiter RD. Role of the Y5 neuropeptide Y receptor in feeding and obesity. *Nat Med*. 1998;4(6):718–721.
21. Minor RK, et al. The arcuate nucleus and neuropeptide Y contribute to the antitumorigenic effect of calorie restriction. *Aging Cell*. 2011;10(3):483–492.
22. Kallio J, et al. Altered intracellular processing and release of neuropeptide Y due to leucine 7 to proline 7 polymorphism in the signal peptide of preproneuropeptide Y in humans. *FASEB J*. 2001;15(7):1242–1244.
23. Hansel DE, Eipper BA, Ronnett GV. Neuropeptide Y functions as a neuroproliferative factor. *Nature*. 2001;410(6831):940–944.
24. Singh P, et al. Neuropeptide Y regulates a vascular gateway for hematopoietic stem and progenitor cells. *J Clin Invest*. 2017;127(12):4527–4540.
25. Moleda L, et al. Amelioration of portal hypertension and the hyperdynamic circulatory syndrome in cirrhotic rats by neuropeptide Y via pronounced splanchnic vasoaction. *Gut*. 2011;60(8):1122–1132.
26. Dietrich P, et al. Dysbalance in sympathetic neurotransmitter release and action in cirrhotic rats: impact of exogenous neuropeptide Y. *J Hepatol*. 2013;58(2):254–261.
27. Hartl J, Dietrich P, Moleda L, Müller-Schilling M, Wiest R. Neuropeptide Y restores non-receptor-mediated vasoconstrictive action in superior mesenteric arteries in portal hypertension. *Liver Int*. 2015;35(12):2556–2563.
28. Sigala B, et al. Sympathetic nervous system catecholamines and neuropeptide Y neurotransmitters are upregulated in human NAFLD and modulate the fibrogenic function of hepatic stellate cells. *PLoS One*. 2013;8(9):e72928.
29. Li L, de La Serre CB, Zhang N, Yang L, Li H, Bi S. Knockdown of neuropeptide Y in the dorsomedial hypothalamus promotes hepatic insulin sensitivity in male rats. *Endocrinology*. 2016;157(12):4842–4852.
30. Ailanen L, et al. The metabolic syndrome in mice overexpressing neuropeptide Y in noradrenergic neurons. *J Endocrinol*. 2017;234(1):57–72.
31. Bruinstroop E, et al. Hypothalamic neuropeptide Y (NPY) controls hepatic VLDL-triglyceride secretion in rats via the sympathetic nervous system. *Diabetes*. 2012;61(5):1043–1050.
32. Becker FF. Inhibition of spontaneous hepatocarcinogenesis in C3H/HeN mice by transplanted hepatocellular carcinomas. *Cancer Res*. 1981;41(9 pt 1):3320–3323.
33. Becker FF, Stillman D, Sell S. Serum α-fetoprotein in a mouse strain (C3H-Avy fB) with spontaneous hepatocellular carcinomas. *Cancer Res*. 1977;37(3):870–872.
34. Heston WE, Vlahakis G, Deringer MK. High incidence of spontaneous hepatomas and the increase of this incidence with urethan in C3H, C3Hf, and C3He male mice. *J Natl Cancer Inst*. 1960;24:425–435.
35. Buchmann A, Bauer-Hofmann R, Mahr J, Drinkwater NR, Luz A, Schwarz M. Mutational activation of the c-Ha-ras gene in liver tumors of different rodent strains: correlation with susceptibility to hepatocarcinogenesis. *Proc Natl Acad Sci U S A*. 1991;88(3):911–915.
36. Jang JJ, Weghorst CM, Henneman JR, Devor DE, Ward JM. Progressive atypia in spontaneous and N-nitrosodiethylamine-induced hepatocellular adenomas of C3H/HeNCr mice. *Carcinogenesis*. 1992;13(9):1541–1547.
37. Lee GH, Sawada N, Mochizuki Y, Nomura K, Kitagawa T. Immortal epithelial cells of normal C3H mouse liver in culture: possible precursor populations for spontaneous hepatocellular carcinoma. *Cancer Res*. 1989;49(2):403–409.
38. Ruebner BH, Gershwin ME, Meierhenry EF, Hsieh LS, Dunn PL. Irreversibility of liver tumors in C3H mice. *J Natl Cancer Inst*. 1984;73(2):493–498.
39. Wolf MJ, et al. Metabolic activation of intrahepatic CD8+ T cells and NKT cells causes nonalcoholic steatohepatitis and liver cancer via cross-talk with hepatocytes. *Cancer Cell*. 2014;26(4):549–564.
40. Chaisaingmongkol J, et al. Common molecular subtypes among Asian hepatocellular carci-

noma and cholangiocarcinoma. *Cancer Cell*. 2017;32(1):57–70.e3.
41. Llovet JM, Burroughs A, Bruix J. Hepatocellular carcinoma. *Lancet*. 2003;362(9399):1907–1917.
42. Dietrich P, Koch A, Fritz V, Hartmann A, Bosserhoff AK, Hellerbrand C. Wild type Kirsten rat sarcoma is a novel microRNA-622-regulated therapeutic target for hepatocellular carcinoma and contributes to sorafenib resistance. *Gut*. 2018;67(7):1328–1341.
43. Hellerbrand C, et al. The novel gene MIA2 acts as a tumour suppressor in hepatocellular carcinoma. *Gut*. 2008;57(2):243–251.
44. Amann T, et al. Reduced expression of fibroblast growth factor receptor 2IIIb in hepatocellular carcinoma induces a more aggressive growth. *Am J Pathol*. 2010;176(3):1433–1442.
45. Huang WY, et al. MethHC: a database of DNA methylation and gene expression in human cancer. *Nucleic Acids Res*. 2015;43(Database issue):D856–D861.
46. Pérez RF, Tejedor JR, Bayón GF, Fernández AF, Fraga MF. Distinct chromatin signatures of DNA hypomethylation in aging and cancer. *Aging Cell*. 2018;17(3):e12744.
47. Mudbhary R, et al. UHRF1 overexpression drives DNA hypomethylation and hepatocellular carcinoma. *Cancer Cell*. 2014;25(2):196–209.
48. Bárcena-Varela M, et al. Dual targeting of histone methyltransferase G9a and DNA-methyltransferase 1 for the treatment of experimental hepatocellular carcinoma. *Hepatology*. 2019;69(2):587–603.
49. Argemi J, et al. Defective HNF4α-dependent gene expression as a driver of hepatocellular failure in alcoholic hepatitis. *Nat Commun*. 2019;10(1):3126.
50. Yamashita T, Wang XW. Cancer stem cells in the development of liver cancer. *J Clin Invest*. 2013;123(5):1911–1918.
51. Nakamura Y, Yanagawa Y, Morrison SF, Nakamura K. Medullary reticular neurons mediate neuropeptide Y-induced metabolic inhibition and mastication. *Cell Metab*. 2017;25(2):322–334.
52. Criscione L, et al. Food intake in free-feeding and energy-deprived lean rats is mediated by the neuropeptide Y5 receptor. *J Clin Invest*. 1998;102(12):2136–2145.
53. Turnbull AV, et al. Selective antagonism of the NPY Y5 receptor does not have a major effect on feeding in rats. *Diabetes*. 2002;51(8):2441–2449.
54. Erondu N, et al. Neuropeptide Y5 receptor antagonism does not induce clinically meaningful weight loss in overweight and obese adults. *Cell Metab*. 2006;4(4):275–282.
55. Schmitz V, et al. Establishment of an orthotopic tumour model for hepatocellular carcinoma and non-invasive in vivo tumour imaging by high resolution ultrasound in mice. *J Hepatol*. 2004;40(5):787–791.
56. Mannon PJ, Raymond JR. The neuropeptide Y/peptide YY Y1 receptor is coupled to MAP kinase via PKC and Ras in CHO cells. *Biochem Biophys Res Commun*. 1998;246(1):91–94.
57. Mullins DE, Zhang X, Hawes BE. Activation of extracellular signal regulated protein kinase by neuropeptide Y and pancreatic polypeptide in CHO cells expressing the NPY Y(1), Y(2), Y(4) and Y(5) receptor subtypes. *Regul Pept*. 2002;105(1):65–73.
58. Nakagawa S, et al. Molecular liver cancer prevention in cirrhosis by organ transcriptome analysis and lysophosphatidic acid pathway inhibition. *Cancer Cell*. 2016;30(6):879–890.
59. Tsuchida T, Friedman SL. Mechanisms of hepatic stellate cell activation. *Nat Rev Gastroenterol Hepatol*. 2017;14(7):397–411.
60. Bataller R, Brenner DA. Liver fibrosis. *J Clin Invest*. 2005;115(2):209–218.
61. Saito Y, et al. Induction of differentiation of intrahepatic cholangiocarcinoma cells to functional hepatocytes using an organoid culture system. *Sci Rep*. 2018;8(1):2821.
62. Nitta T, Kim JS, Mohuczy D, Behrns KE. Murine cirrhosis induces hepatocyte epithelial mesenchymal transition and alterations in survival signaling pathways. *Hepatology*. 2008;48(3):909–919.
63. Ruddell RG, et al. Ferritin functions as a proinflammatory cytokine via iron-independent protein kinase C ζ/nuclear factor κB-regulated signaling in rat hepatic stellate cells. *Hepatology*. 2009;49(3):887–900.
64. Kubes P, Mehal WZ. Sterile inflammation in the liver. *Gastroenterology*. 2012;143(5):1158–1172.
65. Xiang DM, et al. The HLF/IL-6/STAT3 feedforward circuit drives hepatic stellate cell activation to promote liver fibrosis. *Gut*. 2018;67(9):1704–1715.
66. Park MH, et al. Neuropeptide Y induces hematopoietic stem/progenitor cell mobilization by regulating matrix metalloproteinase-9 activity through Y1 receptor in osteoblasts. *Stem Cells*. 2016;34(8):2145–2156.
67. Vial E, Sahai E, Marshall CJ. ERK-MAPK signaling coordinately regulates activity of Rac1 and RhoA for tumor cell motility. *Cancer Cell*. 2003;4(1):67–79.
68. Fredholm BB, Jansen I, Edvinsson L. Neuropeptide Y is a potent inhibitor of cyclic AMP accumulation in feline cerebral blood vessels. *Acta Physiol Scand*. 1985;124(3):467–469.
69. Mukai M, et al. Hepatoma cell migration through a mesothelial cell monolayer is inhibited by cyclic AMP-elevating agents via a Rho-dependent pathway. *FEBS Lett*. 2000;484(2):69–73.
70. Giannelli G, Koudelkova P, Dituri F, Mikulits W. Role of epithelial to mesenchymal transition in hepatocellular carcinoma. *J Hepatol*. 2016;65(4):798–808.
71. Krebs AM, et al. The EMT-activator Zeb1 is a key factor for cell plasticity and promotes metastasis in pancreatic cancer. *Nat Cell Biol*. 2017;19(5):518–529.
72. Giannelli G, Villa E, Lahn M. Transforming growth factor-β as a therapeutic target in hepatocellular carcinoma. *Cancer Res*. 2014;74(7):1890–1894.
73. Rani B, et al. Galunisertib suppresses the staminal phenotype in hepatocellular carcinoma by modulating CD44 expression. *Cell Death Dis*. 2018;9(3):373.
74. Matsuyama S, et al. SB-431542 and Gleevec inhibit transforming growth factor-β-induced proliferation of human osteosarcoma cells. *Cancer Res*. 2003;63(22):7791–7798.
75. Coulouarn C, Factor VM, Thorgeirsson SS. Transforming growth factor-beta gene expression signature in mouse hepatocytes predicts clinical outcome in human cancer. *Hepatology*. 2008;47(6):2059–2067.
76. Zukowska-Grojec Z, et al. Neuropeptide Y: a novel angiogenic factor from the sympathetic nerves and endothelium. *Circ Res*. 1998;83(2):187–195.
77. Wagner L, et al. Identifying neuropeptide Y (NPY) as the main stress-related substrate of dipeptidyl peptidase 4 (DPP4) in blood circulation. *Neuropeptides*. 2016;57:21–34.
78. Ghorpade DS, et al. Hepatocyte-secreted DPP4 in obesity promotes adipose inflammation and insulin resistance. *Nature*. 2018;555(7698):673–677.
79. Fukui Y, Yamamoto A, Kyoden T, Kato K, Tashiro Y. Quantitative immunogold localization of dipeptidyl peptidase IV (DPP IV) in rat liver cells. *Cell Struct Funct*. 1990;15(2):117–125.
80. Drucker DJ, Nauck MA. The incretin system: glucagon-like peptide-1 receptor agonists and dipeptidyl peptidase-4 inhibitors in type 2 diabetes. *Lancet*. 2006;368(9548):1696–1705.
81. Gruenewald DA, Naai MA, Marck BT, Matsumoto AM. Age-related decrease in neuropeptide-Y gene expression in the arcuate nucleus of the male rat brain is independent of testicular feedback. *Endocrinology*. 1994;134(6):2383–2389.
82. Wiest R, et al. Enhanced Y1-receptor-mediated vasoconstrictive action of neuropeptide Y (NPY) in superior mesenteric arteries in portal hypertension. *J Hepatol*. 2006;44(3):512–519.
83. Chiodera P, Volpi R, Pilla S, Cataldo S, Coiro V. Decline in circulating neuropeptide Y levels in normal elderly human subjects. *Eur J Endocrinol*. 2000;143(5):715–716.
84. Delire B, et al. Aging enhances liver fibrotic response in mice through hampering extracellular matrix remodeling. *Aging (Albany NY)*. 2016;9(1):98–113.
85. Richter K, Konzack A, Pihlajaniemi T, Heljasvaara R, Kietzmann T. Redox-fibrosis: impact of TGFβ1 on ROS generators, mediators and functional consequences. *Redox Biol*. 2015;6:344–352.
86. Arrese M, Hernandez A, Astete L, Estrada L, Cabello-Verrugio C, Cabrera D. TGF-β and hepatocellular carcinoma: when a friend becomes an enemy. *Curr Protein Pept Sci*. 2018;19(12):1172–1179.
87. Lv X, et al. Neuropeptide Y1 receptor inhibits cell growth through inactivating mitogen-activated protein kinase signal pathway in human hepatocellular carcinoma. *Med Oncol*. 2016;33(7):70.
88. Park MH, Min WK, Jin HK, Bae JS. Role of neuropeptide Y in the bone marrow hematopoietic stem cell microenvironment. *BMB Rep*. 2015;48(12):645–646.
89. Wang W, Rigueur D, Lyons KM. TGFβ signaling in cartilage development and maintenance. *Birth Defects Res C Embryo Today*. 2014;102(1):37–51.
90. Abou-Alfa GK, et al. A phase Ib, open-label study of dalantercept, an activin receptor-like kinase 1 ligand trap, plus sorafenib in advanced hepatocellular carcinoma. *Oncologist*. 2019;24(2):161–170.
91. Ambrosi TH, et al. Adipocyte accumulation in the bone marrow during obesity and aging impairs stem cell-based hematopoietic and bone regeneration. *Cell Stem Cell*. 2017;20(6):771–784.e6.
92. Thasler WE, Weiss TS, Schillhorn K, Stoll PT, Irrgang B, Jauch KW. Charitable state-controlled foundation human tissue and cell research: ethic and legal aspects in the supply of surgically removed human tissue for research in the academic and commercial sector in Germany. *Cell Tissue Bank*. 2003;4(1):49–56.